Creep of 316L austenitic steel at 450–550 °C in static lead-bismuth eutectic covered by argon-hydrogen gas

Mariya Yurechko*, Aleksandr Skrypnik, Olaf Wedemeyer, Jürgen Konys, Carsten Schroer

Institute for Applied Materials – Applied Materials Physics, Karlsruhe Institute of Technology (KIT) Hermann-von-Helmholtz-Platz 1, 76344 Eggenstein-Leopoldshafen, Germany

ARTICLE INFO

ABSTRACT

Uniaxial creep of the 316L austenitic steel is studied in static oxygen-controlled lead-bismuth eutectic (LBE) with an oxygen content of 10^{-6} wt. % decreasing to 10^{-11} wt. % and in air at 450–550 °C. Dissolution of the steel components (nickel, iron and chromium) in liquid metal with a following formation of a depletion zone and ingress of liquid metal inwards a depleted zone are observed in all LBE-experiments. At 500 and 550 °C, the 316L austenitic steel ruptured much earlier in LBE than in air, while at 450 °C the specimens were still in-tact after long-term testing in LBE (7,178 h) and air (5,783 h). Dissolution of the steel in LBE at 550 and 500 °C is detected to localize close to the failure and unaffected steel surface close to the screw head of the cylindrical creep specimens where creep rate is comparatively low, while at 450 °C, a surface of the whole LBE-specimen is dissolved in liquid metal during a long-term LBE-test. Reference air-specimens show an insignificant surface oxidation at 450–550 °C and creep rate at least one order lower than for the LBE-specimens. Liquid metal embrittlement effect was not observed in 316L tested in LBE.

1. Introduction

The development of Generation IV nuclear reactors and accelerated driven systems (ADS) waked an interest in the compatibility of stainless steels with heavy liquid metal (HLM) under static mechanical load [1,2]. HLMs are represented by lead or lead-bismuth eutectic (LBE) which are foreseen to be used as a coolant and/or spallation target while austenitic steels are considered as a main candidate vessel (316L). However, LBE is corrosive medium especially for austenitic steels, since these steels contain highly soluble element like nickel, while chromium and iron have a lower solubility limit [1]. Dissolution of austenite-stabilizers such as Ni and Mn will cause the phase transformation [3–12]. Dissolution of the steel components in LBE can be delayed if a steel surface will be covered with a stable protective oxide layer. Formation of oxides with the steel elements like Fe, Cr, and Ni takes place under sufficient oxygen supply to the steel surface. But, an oxidation of the steel has to be optimal, so that, on the one hand, the surface is protected from the corrosive medium, and, on the other hand, the steel does not oxidize too fast, so that the construction remains mechanical properties of an original material, for instance creep-to-rupture characteristics. During creep testing, oxides form under

stress applied to the tensile specimen. Therefore, it is to expect an oxide scale growing on the steel surface can tire with crack formation, and in an extreme case split off from the steel surface. If the oxygen concentration of the liquid metal high enough to heal up a new formed victim steel surface, newly formed oxide layer would protect the steel from the dissolution. But it cannot be excluded that a local content of oxygen in LBE at crack tip will be too low to form oxides again, since a significant part of oxygen was consumed earlier. A thin chromium and silicon rich oxide scale was reported for 316L tested in flowing LBE at 550 °C and 10^{-6} wt. % oxygen dissolved in liquid metal for exposure times ≤4000 h, but local selective leaching of Ni and Cr accompanied by ingress of Pb and Bi into the near-surface depleted zone of the steel was observed on the steel after exposure for 2000 h [13]. Therefore, Ar-H_2 gas is used here to simulate critical conditions - low oxygen content of liquid metal under stress as well as $c_o=10^{-6}$ wt.% like edge condition - for study of the 316L steel under creep.

During the last decade of experimental activity, a number of results regarding corrosion behaviour of austenitic steels in HLM were obtained [12,14–19]. However, there is almost no information on creep and stress rupture of austenitic steels in contact with lead or LBE. E.E. Glickman was one of the first to mention a detrimental effect of liquid metals on creep [20].

When steel stressed is in contact with liquid metal, Liquid Metal Embrittlement (LME) may occur, i.e. loss of strength and

* Corresponding author.
E-mail address: Mariya.Yurechko@kit.edu (M. Yurechko).

Table 1
Chemical composition in wt.% of the austenitic steel 316L [35].

Fe	Cr	Ni	Mo	Mn	Si	Cu	V	W	Al
Bal.	16.73	9.97	2.05	1.81	0.67	0.23	0.07	0.02	0.018
C	N	P	S	Ti					
0.019	0.029	0.032	0.0035	0.0058					

ductility. Temperature range of 300–450 °C was reported to result in a brittle rupture of ferritic-martensitic steels, while at temperatures higher than 450 °C plasticity of the steels becomes ductile again in lead contained liquid metal [21–24]. In the case of ferritic-martensitic steel T91/LBE couple, it is widely accepted that adsorption of LBE at crack tips and the resulting weakening of interatomic bonding are the governing mechanisms (see citations [8–19] in Ref. [25]). Both intergranular (interlath) and transgranular (tranthlath) cracking can occur in this couple at 250, 350 and 400 °C [25].

The 15–15Ti(Si) austenitic steel was reported to be studied on creep behaviour in static lead with non-controlled c_o and in air at 550 °C in a stress range of 300–560 MPa [26]. Reduction of creep-to-rupture time and of creep strain was reported for specimens tested in lead in comparison to air [26]. Any significant oxidation of the steel surface for the Pb-tests up to 1200 h was not reported. Recent work on creep with 15–15Ti in LBE at 550 and 600 °C under load of 300 MPa shows degradation of the steel in liquid metal due to dissolution corrosion and especially localized intergranular cracking [27].

To study the LME phenomenon, Slow Strain Rate Tensile (SSRT) tests were carried out for the AISI 316L/LBE couple [28]. Any major effect due to intimate contact of the irradiated austenitic stainless steel 316L with LBE was found. In other fracture-toughness-studies the authors came to conclusion that the mechanism of LME in general is still a matter of debate and mechanical properties of the 316L austenitic steel are not clearly affected by the presence of LBE in comparison to ferritic steel T91 [29,30].

In this work, the effect of static, oxygen controlled lead-bismuth eutectic (LBE) with $c_o \le 10^{-6}$ wt. % on creep properties is examined in the temperature range from 450 to 550 °C and loading range from 300 to 375 MPa in comparison to air.

2. Experimental

2.1. Sample material, specimen preparation

The chemical composition of the austenitic Cr-Ni-Mo steel 316L is presented in Table 1. The microstructure of the as-received steel contains lamellae at grain boundaries of austenitic grains (Fig. 1a,b). Auger electron spectroscopy indicates an enrichment in chromium and clear depletion of nickel for these lamellae in contrast to the average composition of the 316L matrix (Fig. 1c,d), which implies δ-ferrite. δ-Ferrite can form as a second phase in austenitic matrix during solidification/fabrication and remains stable in the temperature range up to 1400 °C. Solution annealing of the steel at 1050 °C does not lead to the dissolution of the secondary phase. For the same steel as ours it was determined that some chemical banding with Ni fluctuation over hundreds of μm at the % level [31], while other authors revealed that formation of the δ-ferrite affected by the steel chemical composition, and less affected by the cooling rate [32]. Schaeffler diagrams basing on ratio of the alloying elements (chromium, nickel etc.) that stabilize ferrite and austenite help to foresee formation of ferrite in austenitic matrix [33].

Cylinders for the creep specimens with a basic geometry conform to DIN EN ISO 204:209 [34] presented in Fig. 2 have been cut from the heat-treated steel plate in a rolling direction by electric discharge machining with a subsequent turning. Finally, the speci-

mens have been cleaned with acetone in ultrasonic bath and dried in ambient air.

Before the specimen was built-in the capsule for testing, its actual size was determined in a contact-free manner with a laser scanner with spatial resolutions of 0.1 mm and 1 μm for the length *Lc, Lo* and gauge diameter *Do* (Fig. 2), respectively. Cylindrical specimens are measured in their as-received state by rotating of 90 ° in the angle range from 0 to 270°, so that an ovality of every specimen can be excluded. Both parts of the same specimens after rupture are measured by rotating of 30° and 0.1 mm close to the failure so that the whole length of the ruptured specimen can be reconstructed. Non-ruptured specimens after the testing were measured in the same manner so that the measuring results can be direct compared.

LBE-specimens before dimension measurements were cleaned from liquid metal in a bath with hot glycerine at about 150 °C. If some liquid metal was remained on the failure surface afterwards, the specimen was cleaned additionally with a CH_3COOH-H_2O_2-solution (1:1). The 316L-specimen tested in LBE at 550 °C and $c_o = 10^{-6}$ wt.% ($t_R = 371$ h) was exceptionally not cleaned, so that corrosion processes could be studied in respect to microstructural changes in the steel surface and its vicinity in liquid metal.

Reduction of the load-bearing cross-section during the testing, a thickness of corrosive layer and structural changes in the surface were measured in a post-test state of the specimen on the transversal cross-section cut from the gauge length, *Lc* 1 cm away from the specimen shoulder.

The regularity of all changes was studied on the elongated cross-section cut from the ruptured part beginning from the place where the transversal cross-section was cut, up to the failure.

2.2. CRISLA facility, pre- and post-test analyses

The measured specimens are encapsulated both in stagnant LBE and in air. The capsules for the tests in oxygen-contained stagnant LBE contain 0.9 l of liquid metal, while the volume of the capsules for testing in air is about 0.23 l. The flexible bellows on the lid of the capsule allowed for elongation of the specimen, i.e. creep deformation. The elongation was measured and recorded as a function of time via the movement of the pulling rod, outside the capsule, since corrosion of extensometer in liquid metal would lead with a time to incorrect measuring data and engine trouble of the whole measuring system. All extensometers were checked on their characteristics/parameters on the corresponding test stand with a standard specimen installed into the working stand in air at room temperature by means of measuring cell. Since a cross-section diameter of the tensile specimen is much lower than any part of the pulling equipment, a measured elongation was assumed to result in measured elongation of the tested specimen. It was taken in account a potential elongation of the whole pulling section between the specimen and the extensometer due to its re-arrangement in a straight line during the full loading. Therefore, the data during the first minute after the test start is removed from the elongation curve. Our measurements data allow us, to compare data for the different surrounding systems (air, liquid metal etc.) and make a conclusion on an effect of the liquid metal at high temperatures and different oxygen content in comparison to air for the same material.
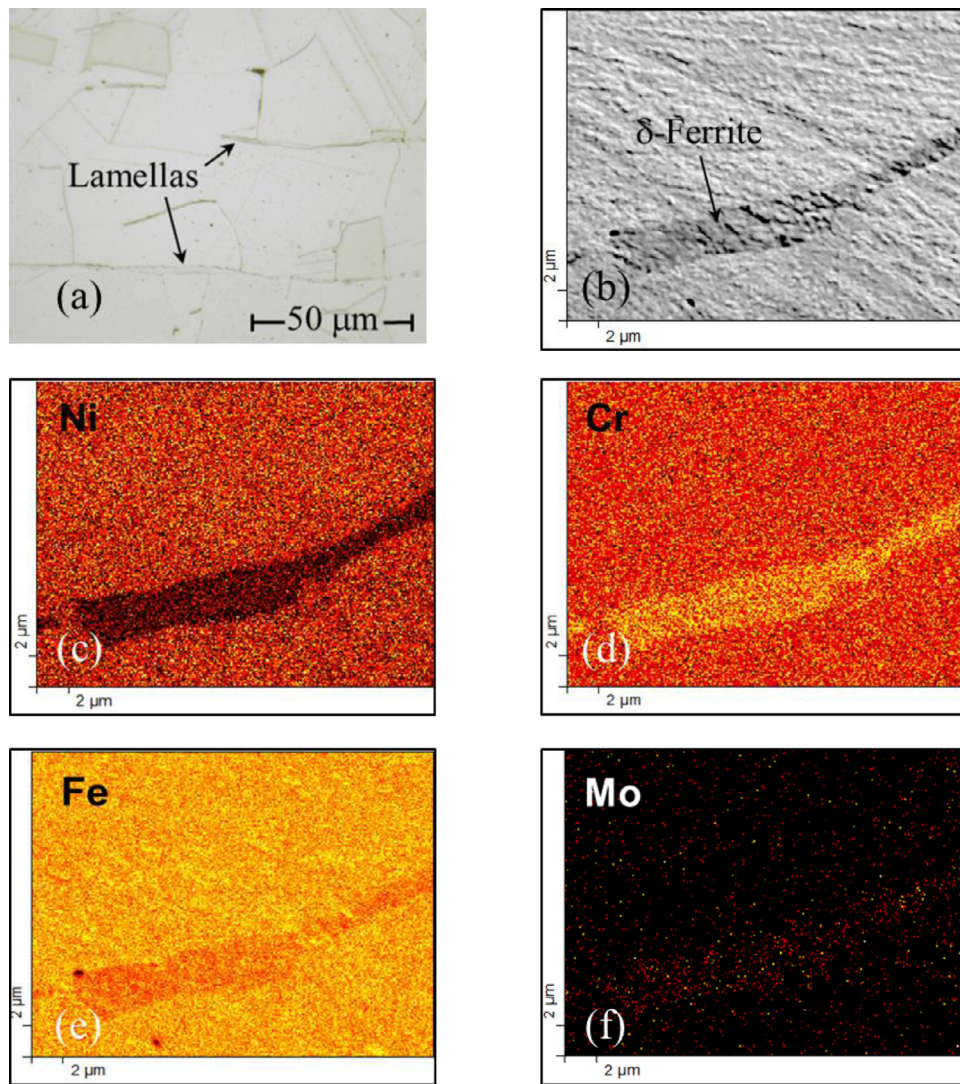
Fig. 1. (a) Optical microscopy image and (b) SEM-image of the 316L austenitic steel in as-received state; (c-f) Auger electron spectroscopy mapping of the same place presented on (b) for Ni, Cr, Fe and Mo elements.
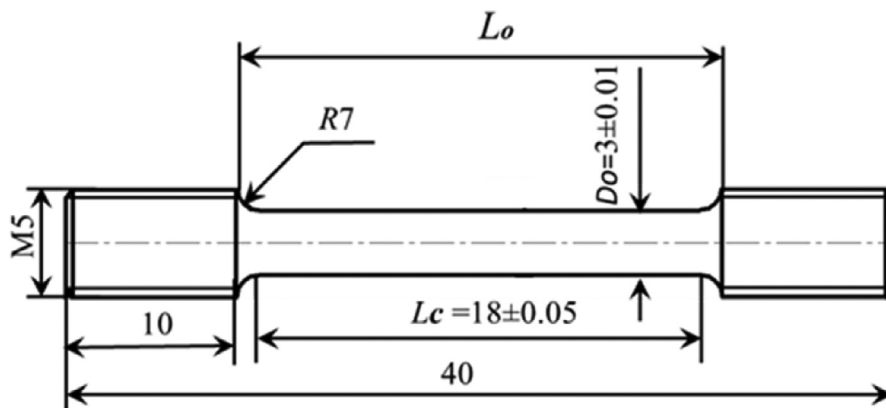

Fig. 2. Workshop drawing of the used specimens with a basic geometry conform to DIN EN ISO 204:209.

The capsules with liquid metal and air are parts of the CRISLA facility [36] with oxygen control performed with oxygen-contained gases [37]. The capsules for tests in LBE contain approximately 9 kg of the liquid metal. The gases (Ar, Ar-5 vol.% H$_2$ and synthetic air) are introduced into LBE via tube in the lid with though the gas/liquid metal phase. Creep test starts as soon the temper-

ature reaches 500 °C and oxygen sensor shows E > 965 mV that corresponds approximately $c_o=10^{-6}$ wt.% for the tests with LBE at 550 °C. Sometimes depending on the capsule a working schedule is not long enough to reach this oxygen-sensor voltage. Therefore, there are some cases when the specimen was loaded shortly before an oxygen concentration reached the goal value. Creep tests in LBE
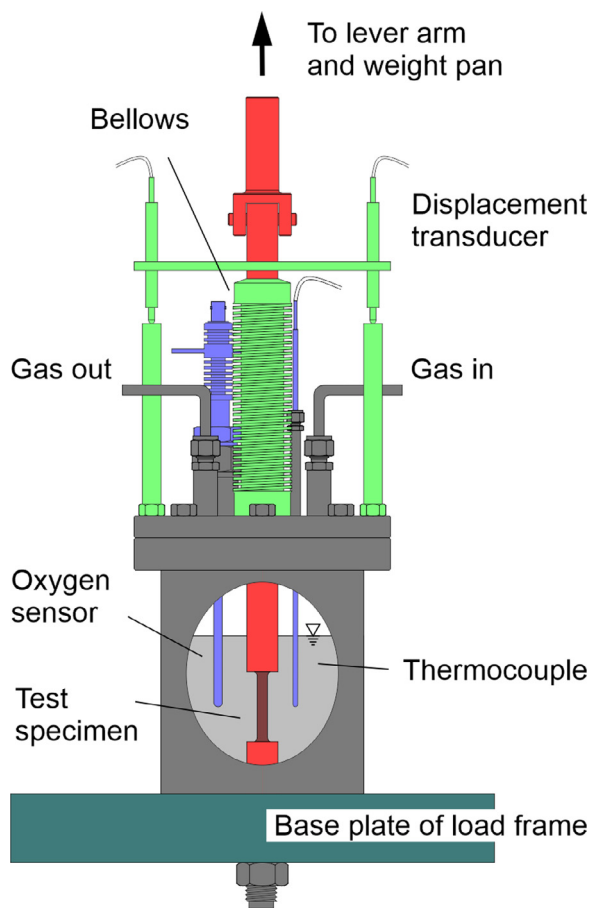
Fig. 3. Scheme of elongation measurements with two displacement transducers.

with decreasing oxygen concentration were carried out with a goal to reach an oxygen concentration in liquid metal as low as possible and imitate a potentially real situation with a lowering of the oxygen content in LBE. Supply volume rate of all gases during a creep experiment as soon as c_o reaches 10^{-6} wt. % is: 96 ml/min carrier gas Ar, 3 ml/min Ar-5 vol.% H_2 and 1 ml/min synthetic air. Since the whole system with liquid metal is very sensitive, supply volume of the gases can be slightly changed. Nevertheless, total volume of gases remains around 100 ml/min. By experiments with a lowering of oxygen dissolved in liquid metal, only Ar-5 vol.% H_2 is supplied permanently with 100 ml/min. There are some cases when preparation of the experiment before it can be started is longer than a working day, so that such experiments can be started shortly before the oxygen content reaches goal value like it was in Fig. 5. Tests with lowering of oxygen dissolved in LBE were carried out so that tests reflect a real situation with change of an oxygen content on the one hand. On the other hand, if one waits around 600 h until the oxygen content will be stabilized at 650 °C like it would be in Fig. 4, the specimen could get strong changes in microstructure, resulting in loss of the mechanical properties with a following rupture immediately after the full loading. Further details for the control of oxygen content is presented in Ref. [38].

The specimen elongation was measured during the test with two displacement transducers fixed outside the capsule, on two sides of the pulling rod (Fig. 3), so that their connecting metallic plate is perpendicular to the level arm connected to the weight pan. Two transferring plates of the corresponding displacement transducers are fixed on the facility frame. The measurements are recorded every 1 minute. For long-term tests, the mentioned recording frequency is used only for the first few hours of the test

with a further frequency of 1 point/1 hour. Considering the order of starting the displacement recording and loading the specimen, the measured absolute displacement contains the elastic deformation of the specimen and the loading system. It is assumed that these deformations are contained in the first value recorded after 1 minute, with a negligible part going back to creep of the specimen during the first minute. Two displacement curves obtained from the two displacement transducers are recalculated in the average one for the further analysis.

The concentration of oxygen dissolved in the provided LBE volume was monitored by (Pt)/air oxygen sensor close to the specimen centre under permanently supply of Ar-5 vol.%H_2 with a rate of 100 ml/min. In some of the tests where oxygen concentration was target at 10^{-6} wt.% by introducing either oxygen-rich or oxygen-lean gas, depending on the measured oxygen concentration at a moment. Hereby, all experiments are characterized by the sensor output, E and c_o as a function of testing time. Temperature measured close to the specimen centre inside of the capsule surrounded with LBE or air was measuring with Ni-NiCr thermocouple. The actual investigation plan and all data measured in situ as well as oxygen concentration in LBE recalculated from the sensor output are presented for the main experiments in LBE at 550, 500, 450 °C and uniaxial tensile stress in the range of 300–375 MPa (Table 2) similar to T91 [38].

An oxygen concentration of LBE was recalculated using an (Pt)/air oxygen sensor output and the liquid metal temperature measured in-situ corresponding to [39]:

$$\log(c_o/wt.\%) = -3.2837 + \frac{6949.8}{T/K} - 10080 \frac{E/V}{T/K}, \qquad (1)$$

where T is liquid-metal temperature inside the capsule in degrees Kelvin and E is sensor output as indicated by a high-impedance voltmeter in Volts.

Some of the long-tests were stopped before the specimen was ruptured, since any evidence for a rupture in a near future was not detected.

Two examples of test temperature, sensor output and oxygen concentration developing during the tests are presented for two 316L specimens tested in LBE with a lowering of dissolved oxygen and $c_o=10^{-6}$ wt.% at 550 °C in Fig. 4 and Fig. 5, respectively.

At all temperatures, LBE-tests were carried out by lowering oxygen dissolved in liquid metal so that steel elements dissolution was intensified and the specimen rupture would appear in the foreseeable future. To analyse whether a c_o-increase leads to a steel oxidation and, correspondingly, to a longer time-to-rupture in comparison to the low oxygen concentration, three creep-to-rupture tests were done in LBE at constant oxygen concentration ($c_o=1 \times 10^{-6}$ wt.%) and 550 °C, LBE was pre-conditioned every time inside the test capsule in the temperature range of 550–650 °C depending on a dynamic of reduction reaction without any specimen inside. Pre-conditioning time was varying from three days up to one week with a following holding time around 1–2 days as soon as the sensor output reaches 1 V. Thereupon liquid metal was cooled to around 150–200 °C so that LBE was still liquid and a tensile specimen was installed into the capsule under fume hood conditions (in air at normal pressure). A relatively low temperature of LBE and short time when the capsule is open (around 10–15 min) during the specimen will be installed result in a shorter time of heating before the specimen will be fully loaded. The creep specimen is minimal pre-oxidized if at all. This assumption is assisted with post-exposure investigations.

As soon as the capsule with a specimen inside was closed, installed into a test stand, the specimen was pre-loaded with up to 10% of the test load corresponding to ASTM Standards E 139–00 to improve the axiality of loading and heated up to test temperature. As soon as the temperature reached and stabilized by the

Table 2
Test matrix of the creep tests with austenitic steel 316L in low oxygen containing LBE and air at 450–550 °C.

Test medium	Temperature, °C	Load, MPa	Oxygen concentration in liquid metal, wt. %	Test time (stopped * or ruptured, h)
LBE	550	300	1×10^{-7} to 8×10^{-11}; 8×10^{-11} after 400 h	1060
			1.0×10^{-6}	271
			1.0×10^{-6}	182
			1.0×10^{-6}	371
Air			–	1150 *
LBE	500	325	1×10^{-8} to 1×10^{-11}	4996
Air			–	15,226*
LBE	450	375	1×10^{-9} to 1×10^{-10}	7178*
Air			–	5783*

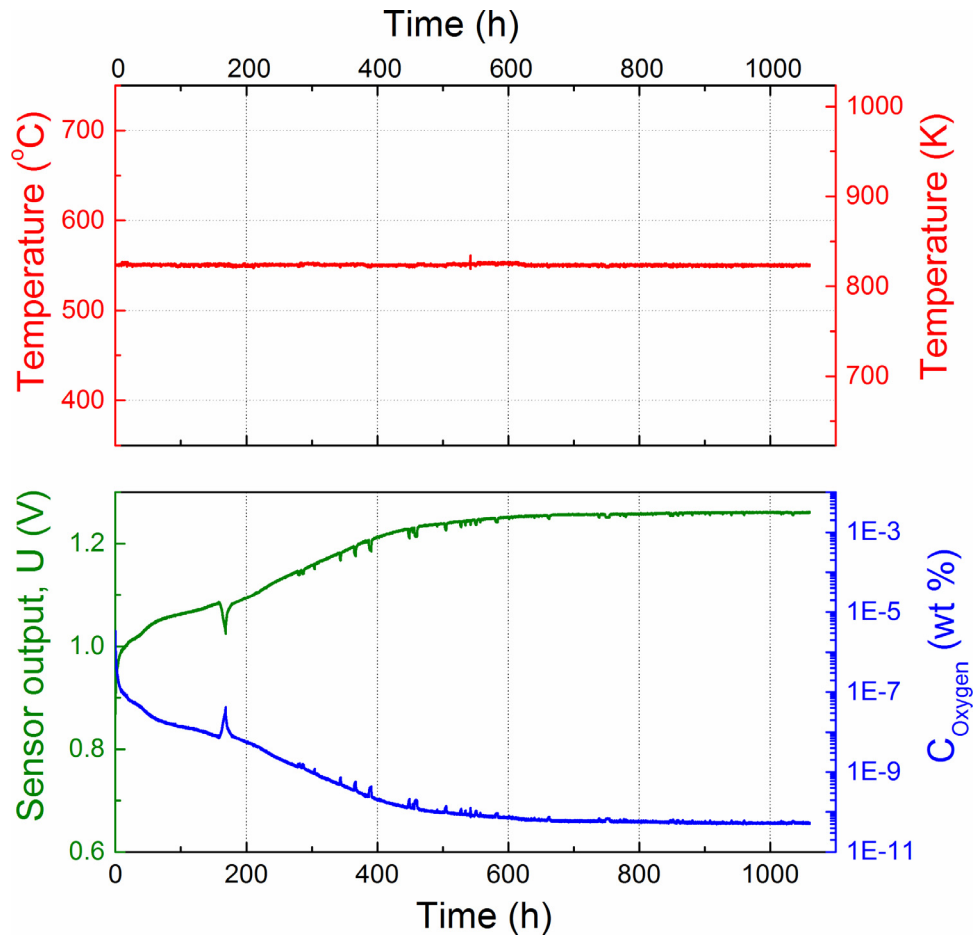* - The creep test was stopped before the specimen was ruptured.

Fig. 4. Temperature, oxygen sensor output measured in-situ and calculated oxygen concentration during the test of 316L crept in LBE at 550 °C up to rupture.

test temperature and sensor output reached 1 V, the full test load was applied to the specimen. A moment of the full loading of the specimen corresponds to the start of the experiment, $t_o = 0$ h. All reference creep tests were carried simultaneously in air at 550, 500 and 450 °C and were interrupted at the same time (at 450 °C) or later than the corresponding tests in LBE (at 550 and 500 °C).

Measurements of the specimen size before and after the test allow to determine creep characteristics of the steel depending on the surrounding media.

The measured initial diameter Do, length Lc and shoulder length Lo were applied to determine sampling length Lr and strain ε_r according to DIN EN ISO 204:209.

$$Lr = Lc + 2 \sum_i \left[(Do/d_i)^{2n} l_i \right], \tag{1}$$

where n is the stress exponent in Norton's law of the material tested and was assumed to be 5 corresponding to Ref. [40] for estimating Lr corresponding to DIN EN ISO 204:209. l_i is the length increment with diameter d_i along the transition between gauge and screw thread of the specimen.

Strain ε_r was calculated from elongation, ΔL measured during the testing as a function of time corresponding to:

$$\varepsilon_r = \Delta L / Lr \times 100 (\%). \tag{2}$$

An engineering strain calculated on the initial gauge diameter, Do, is used in the actual study. Strain at rupture, ε_r^R is a particular case of engineering strain at rupture moment that is determined from the initial length Lr and the total elongation of the specimen after the rupture, ΔL_R:

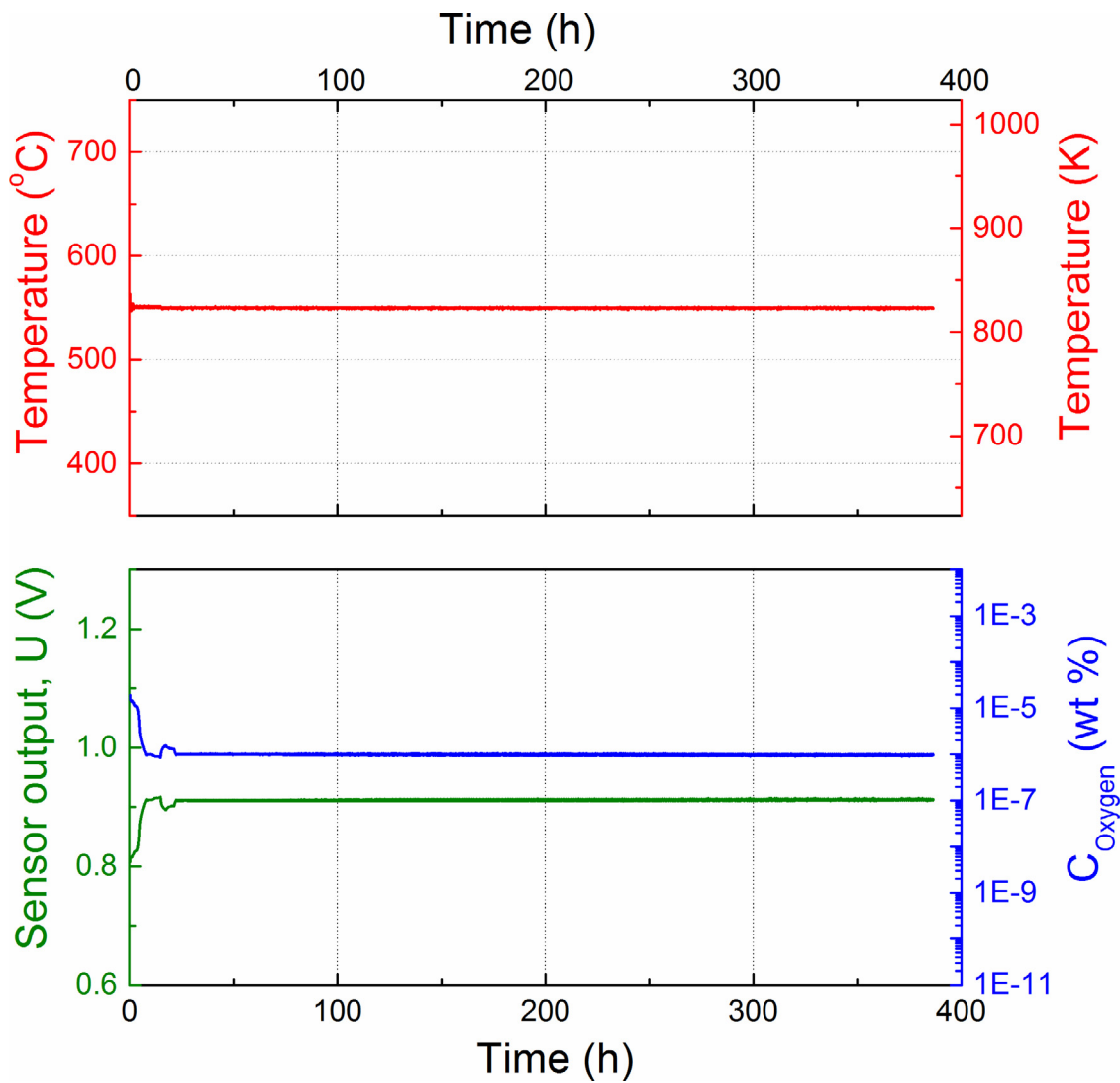$$\varepsilon_r^R = \Delta L / Lr \times 100 (\%), \tag{3}$$

Fig. 5. Temperature, oxygen sensor output measured in-situ and calculated oxygen concentration of 316L crept in LBE with $c_o=10^{-6}$ wt.% at 550 °C up to rupture.

During the creep testing gauge diameter reduces with a time that leads logically to a strain increase with a following reduction of time-to-rupture. Potential factors leading to the *Do*-decrease are creep by itself as well as corrosion of the steel, either oxidation or solution in the liquid metal.

The creep characteristics like the steady-state (minimum) creep rate, $\dot{\varepsilon}_s^r$, times corresponding to the transitions from primary to secondary, $t_{1,2}$, and secondary to tertiary creep, $t_{2,3}$, as well as the time-to-rupture, t_R, were determined from the strain-vs.-time curves as previously described in Ref. [36].

The necking of the specimen after rupture is determined from the initial diameter, *Do* and the smallest diameter after the rupture, D_R by direct measurement on the specimen by means of laser scanner at room temperature:

$$Z/\% = (D_o^2 - (D_R)^2) \times 100/D_o^2, \quad (4)$$

Steel crept in a highly corrosive liquid metal (LBE) extends under load applied as well as corrodes in LBE. Therefore, a specimen diameter measured after the experiment in LBE, D_t or D_R, contains two constituents: reduced cross-section due to specimen elongation with a subtraction of corroded material (D_t is a specimen diameter after the experiment, when the experiment was stopped and the specimen is still intact). This value is referred to as reduction of load-bearing cross-section below (e.g. in Table 3).

Areas close to the failure of ruptured specimens are practically free from momentous corrosion that can be determined by means of SEM, since the corrosion scale tears and detaches rather than deforms under loading. Time of the tertiary zone up to failure, $t_{2,3} \rightarrow t_R$, depends on a material: ductile material is characterized with a longer tertiary zone than a brittle one. Even when this time long enough that corrosion can take place again, formation of the compact layer is rather difficult due to rapid deformation in the necking area. So, a diameter of the gauge length after rupture, D_R that may include a thin and non-compacted corrosion layer is determined with a measurement accuracy of the laser scanner.

2.3. Metallographic study

The tested specimens were studied with a light optical microscopy (LOM) to obtain information on effect of liquid metal on the steel surface as well as scanning electron microscopy (SEM) supplemented by EDX (energy-dispersive X-Ray) analysis to qualify changes in inner of the steel and in the upper surface of the specimen contacted to air and liquid LBE. For it, one piece of the ruptured specimen was used to examine a fracture with SEM, while counter piece was used to produce longitudinal and transversal polished cross-sections and study them with OM, SEM and EDX analysis. To find changes in the microstructure of the steel affected

Table 3
Creep characteristics of the austenitic steel 316L crept (-to-rupture) in oxygen-controlled LBE environment with different c_o and air at 450–550 °C.

Test temperature, °C/ Load, MPa	Test medium	Test time, h	ε_r^R, %	Z, %	$\dot{\varepsilon}_s^r$, h^{-1}	$t_{1,2}$, h	$t_{2,3}$, h	Thickness of a depletion zone, μ	Reduction of sample radius, μ	Reduction of load-bearing cross-section, %
550 / 300	LBE	1060	14.1	29.4	8.0×10^{-5}	34.9	545	168.9	326,4	39
		182	29.3	–	–	–	–	46.4	275.9	33
		231	20.0	31.9	1.6×10^{-3}	19.6	111.8	43.5	201.5	25
		371	14.2	32.2	6.9×10^{-4}	70.9	188.6	6.3	90.3	11.7
	Air	1150*	–	–	8.4×10^{-4}	382.0	>1150	–	–	–
500 / 325	LBE	4996	13,0	43.1	1.5×10^{-5}	146	3162	81.4	283	34
	Air	15,226*	–	–	8.8×10^{-8}	7550	>15,128	–	–	–
450 / 375	LBE	7178*	–	–	1.7×10^{-6}	124.5	–	173	283.3	33.8
	Air	5783*	–	–	5.6×10^{-8}	–	–	–	135.9	–

* - The creep test was stopped before the specimen was ruptured.

by the temperature and corrosive LBE during the testing, the as-received and post-tested states were compared. A mixture of concentrated mineral acids consisting of 30 ml of 32% hydrochloric acid, 10 ml of 65% nitric acid and 5 drops of 97% sulphuric acid was used for the etching of the polished specimens for microstructural study by means of LOM.

The metal loss due to corrosion of the steel and thickness of corrosion layer were measured by means of a digital LOM, so that the quantitative outcome of the interaction of 316L with oxygen-containing stagnant LBE was characterized. So, a transversal polished cross-section of specimens was evaluated with respect to the percentage of sub-surface affected by corrosion. The thickness of corrosion scale as well as reduction of load-bearing cross-section are measured with the Keyence digital LOM turning a vertical cross-section of the specimen after the creep testing around every 15° from 0 till 165°

3. Results

3.1. 550 °C and 300 MPa

The steel tested in LBE at 550 °C and low c_o is characterized with a strain at rupture, $\varepsilon_{r;R}$=14 % at t_R=1060 h (Fig. 6a and Table 3). Steady-state strain rate, $\dot{\varepsilon}_s^r$, defined by the slope dε/dt, is 8.0×10^{-5} h^{-1} as well as the times $t_{1,2}$ and $t_{2,3}$ are determined from the curve to be 34.9 h and 545 h, respectively.

Comparative curves of all 316L-speimens tested at 550 °C and 300 MPa are presented in Fig. 7. All LBE-specimens independent on oxygen dissolved in liquid metal ruptured before the air-specimen. The test in air was stopped after the specimen in LBE at c_o=10^{-7}–10^{-9} wt.% was ruptured (Fig. 6b). The strain-vs.-time-curve of the air-specimen shows no change into the tertiary zone, i.e., $t_{2,3}$ cannot be determined and no evidence of necking was measured in-situ. An increase of oxygen content in LBE up to 10^{-6} wt. % does not improve time-to-rupture, t_R as well.

In LBE under Ar-5 vol.% H_2 cover gas, 316L shows a ductile fracture and well-observed necking after the rupture (Fig. 8a and Fig. 9a). The fracture angle is about 45° to the tensile load direction. The SEM examination of the fracture reveals elongated dimples with their long axis aligned to the tension force direction (Fig. 8b).

A thick corrosion scale is well-observed close to the specimen failure (ferrite in Fig. 8a,c). A depletion zone/ferrite observed in a transversal cross-section is regular and around 168.9 μm (Fig. 10), while its thickness varies significantly along a tensile direction (Fig. 9a). Similar results obtained for other LBE-specimens are described below. Therefore, a thickness of a depletion zone, reduction of sample radius / load-bearing cross-section, presented in Table 3, are snap-shot results and do not illustrate a real corrosion appearance under loading. A depletion zone on the LBE-specimen
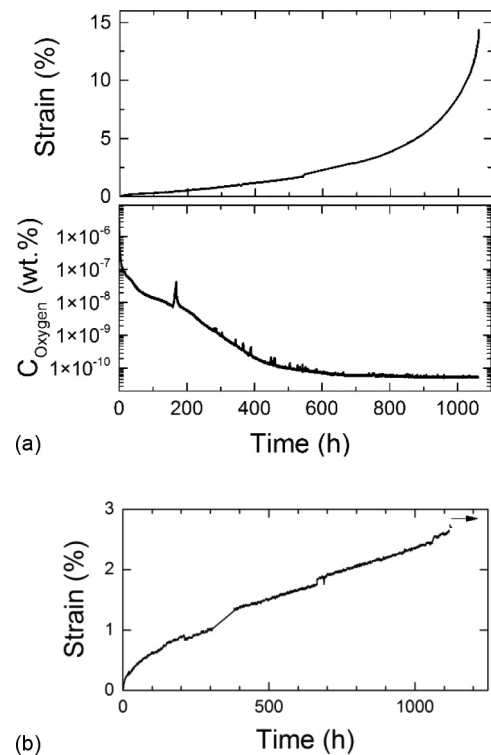

(a)

(b)

Fig. 6. Strain and oxygen output obtained from 316L tested at 550 °C and 300 MPa: (a) in LBE with decreasing c_o, t_R=1060 h and (b) in air (stopped after 1150 h).

is thicker, the closer failure is. But the lateral steel surface close to a failure is free from the depletion zone; a corrosion scale is detached locally on a great area around a failure.

In spite of a great amount of cracks in a depletion zone close to failure, any crack propagation into the steel inwards was not observed in the tested specimen (Figs. 8a, 9b and 10). Some cracks in a corrosion scale are filled with a solidified LBE, some of them not (Fig. 9b). The later do have obviously any direct contact to liquid LBE. Corrosion scale can lose its compactness like in Fig. 10 and liquid metal can touch the steel directly.

A depletion zone shows a lower nickel- and chromium-content in comparison to the steel matrix that is an indication of ferrite formation (Fig. 11). The outer part of a depletion zone with porous, spongy structure contains a relatively high amount of solidified liquid metal (lead and especially bismuth in Fig. 11). Liquid metal is penetrated also deeper into the inner part of a depletion zone, but with a distinguishably lower amount.

Reference specimen tested simultaniously in air at 550 °C was still intact after 1150 h testing as well as experimental data shows
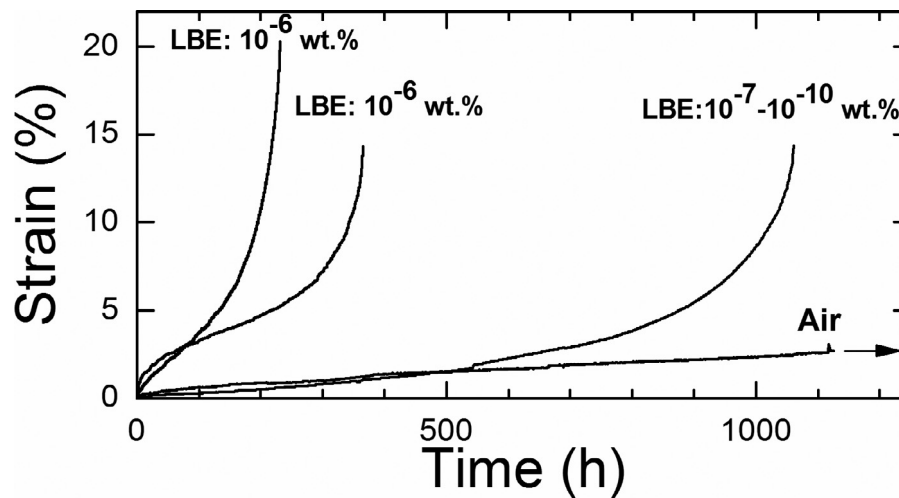
Fig. 7. Strain of 316L crept up to rupture in LBE at low c_o (=10^{-7}–10^{-10} wt.%) and 550 °C. Reference creep(-to-rupture) test is presented through the test in air and in LBE at c_0=10^{-6} wt. %. The test in air was stopped simultaneously with the specimen ruptured in LBE with low oxygen content.
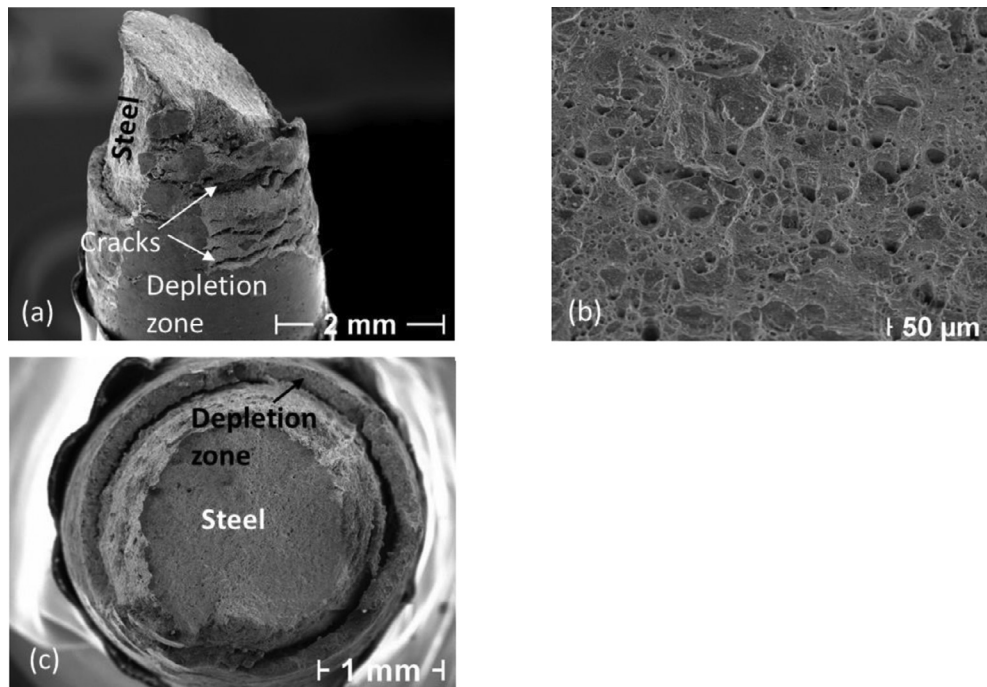

Fig. 8. 316L steel after creep-to-rupture test in LBE with c_o=1×10^{-7}–8×10^{-11} wt.% at 300 MPa and 550 °C for 1060 h: (a-b) sidelong view of the ruptured specimen (a-b); (c-d) top view of the ruptured specimen.

no change in the steady-state strain rate for this specimen. Engineering strain is around 3% after 1150 h (Fig. 6, 12 and Table 3). testing is around 2 %, a steady-state strain rate is 8.4×10^{-5} h^{-1}, and the times $t_{1,2}$ and $t_{2,3}$ are 382 and >1150 h (Fig. 7 and Table 3).

Surface appearance of non-ruptured air-specimen was changed from metallic glossy into dark dull colour after the creep test for 1150 h under 300 MPa. Lateral surface was slightly oxidized, and turning traces occurred during specimen manufacture are still well observed (Fig. 12a). No relevant cracks in the steel surface were detected. Reduction of the load-bearing cross-section around 106 μm occurred rather due to creep than corrosion process.

Any relevant corrosion scale was observed onto steel surface (Fig. 12b). 316L tested in LBE at 550 °C and c_0=10^{-6} wt.% exhibits a rough surface with a numerous cracks almost on the whole gauge length Lc observed by means of an OM and SEM (e.g. Fig. 13a).

Fracture surface exhibits elongated dimples on two surface planes fractured at 45° to the pull direction (Fig. 13b).

Corrosion layer is well definable on the transversal and longitudinal cross-sections of 316L ruptured after 182 h in LBE (Fig. 14). In contrast to 316L tested in LBE with low c_o and t_R=1060 h described above, a depletion zone observed on the steel at constant c_0=10^{-6} wt.% and 182 h is much thinner. Additionally, a depletion zone formed during creep-to-rupture test varies in a thickness as well as a local dissolution of a depletion zone is well observed on the transversal cross-section (Fig. 14c). Few areas without depletion zone are still can be found on the both cross-sections, i.e. diffusion of the steel elements outwards into the liquid metal and vice versa appears irregularly or rather starts locally and distributes with a testing time.

Two other specimens tested at 550 °C, 10^{-6} wt. % dissolved oxygen with t_R=231 and 371 h show similar characteristics of a de-
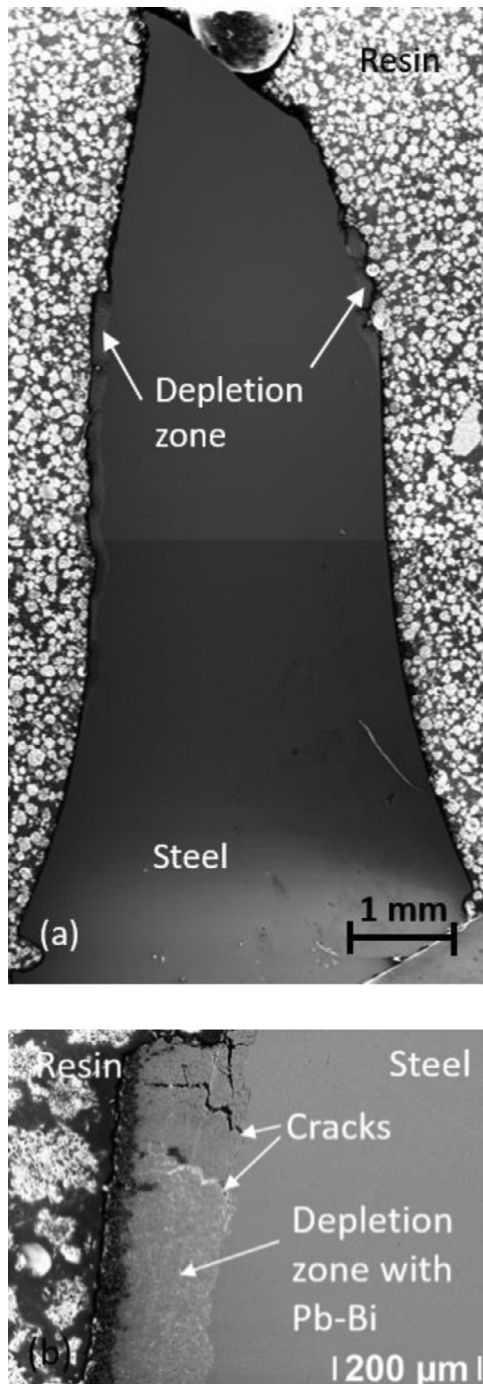
Fig. 9. Longitudinal non-etched cross-section of the 316L-specimen tested in LBE with $c_o=1 \times 10^{-7}$–8×10^{-11} wt.% at 550 °C and 300 MPa and ruptured after 1060 h testing.

pletion zone with 316L tested at low c_o: a depletion zone is significantly thicker for these two specimens in comparison to the case t_R=182 h, but a depletion zone formed during the testing covers the steel surface not completely (Fig. 15a for t_R=371 h).

Both specimens exhibit cracks in a depletion zone filled with LBE (Fig. 15b). Maximal thickness of a depletion zone measured on a longitudinal cross-section of 316L with t_R=231 and 371 h ($c_o=10^{-6}$ wt.%) is approaching to that at low c_o and was measured around 150 μm.

Locally, an oxide layer was formed on top of a depletion zone close to a specimen shoulder that was not cleaned from the so-lidified liquid metal after testing (Fig. 15c). Additionally, oxides of the steel elements were found precipitate in the liquid metal, at steel/depletion zone interface and in a depletion zone filled with LBE (Fig. 15d,e).

Three specimens tested in LBE at 10^{-6} wt.% dissolved oxygen (t_R =182, 231 and 371 h) show strain-at-rupture, ε_r^R by 29.3, 20.0 and 14.2 %, respectively (Fig. 7 and Table 3). A steady-state strain rate, $\dot{\varepsilon}_s^r$ for the specimens tested in LBE with $c_o=10^{-6}$ wt.% (t_R =231 and 371 h) are 6.9×10^{-4} till 1.6×10^{-3} h^{-1} (Table 3). For the both LBE-specimens with $c_o=10^{-6}$ wt.%, times corresponding to the transitions from primary to secondary creep, $t_{1,2}$, are 19.6 and 70.9, and from secondary to tertiary creep, $t_{2,3}$ are 111.8 and 188.6 h (Table 3).

Failure of the LBE-specimens with t_R=182 and 231 h studied with SEM is presented through two shear-face tensile planes at about 45° to the tensile direction (macroscale ductile). The microscopic examination of the fracture reveals elongated dimples similar to the specimen tested at low c_o (Fig. 13b). Therefore, 316L in LBE at 10^{-6} wt.% dissolved oxygen ruptured in a ductile modus similar to that at $c_o=1 \times 10^{-7}$- 8×10^{-11} wt.%.

A thickness of a depletion zone with different oxygen contents was found to vary. The highest thickness of it was determined in the test with a lowering c_o after 1.060 h testing (168.9 μm), while specimens tested in LBE at 10^{-6} wt.% dissolved oxygen exhibit an irregular depletion zone from 0 up to 46 μm after 182, 231 and 371 h (Table 3).

3.2. 500 °C and 325 MPa

The steel 316L tested in LBE with low c_o at 500 °C ruptured after 4996 h testing, while the creep test with the steel in air was stopped after 15,226 h before the specimen was ruptured. The transition time from the secondary to tertiary creep stage, $t_{2,3}$ was not reached, i.e. time-to-rupture in air exceeds more than three order of t_R in LBE (Fig. 16 and Table 3). Steady-state strain rate determined for the LBE-specimen is two orders higher than for the air-specimen: $\dot{\varepsilon}_s^r$ =1.5×10^{-5} h^{-1} in LBE and $\dot{\varepsilon}_s^r$ =8.8×10^{-8} h^{-1} in air. Thereby a significant effect of LBE on creep properties of the 316L austenitic steel in comparison to air is obvious.

SEM/EDX examination of the ruptured specimen tested in LBE with an oxygen concentration between 1×10^{-8} and 1×10^{-11} wt.% showed depletion zone and cracks formed inside, strong necking (43%) and dimples in the fracture after 4996 h testing time (Fig. 17). Failure appearance of this specimen is similar to a macroscopic view of the 316L tested at 550 °C and $c_o \leq 10^{-6}$ wt.%. Fine differences are presented through a little bit more complicated fracture surface with a few planes at 45° to the tensile direction occurred at lower test temperature and longer t_R. Tensile grooves were observed on the lateral steel surface surrounding the failure along the tensile direction (Fig. 17a,b). In addition to the corrosion scale, the specimen exhibits a rough steel surface since a depletion layer detached the steel surface under load and probable due to dissolution of the depleted layer (Fig. 17d).

Regularity of a depletion zone is well observed on the longitudinal and transversal cross-section (Fig. 18). Depletion zone observed on the lateral side of the transversal cross-section is irregularly thick. On a longitudinal cross-section, a depletion zone is much thicker than on the left side (Fig. 18a). A thick depletion scale on the right side is characterized with deep cracks elongated until the steel and filled with the liquid metal like it is presented in Fig. 18c. «Longitudinal» cracks filled with LBE are observed in a depletion zone along tensile direction as well, i.e. these cracks appear during the creep testing and can result in a partial or complete detached of the corrosion scale from the steel surface. It is very possible that this effect is observed on the left side of the longitudinal cross-section and possible under longer t_R than at 550 °C.
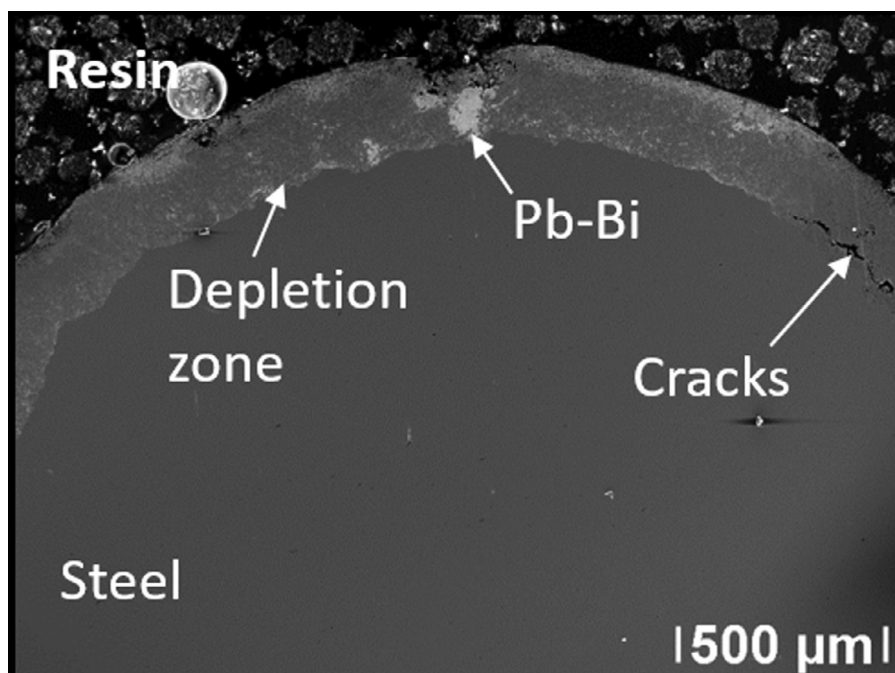
Fig. 10. Transverse non-etched cross-section of the 316L-specimen tested in LBE $c_o=1 \times 10^{-7}$–8×10^{-11} wt.% at 550 °C and 300 MPa and ruptured in 1060 h testing.
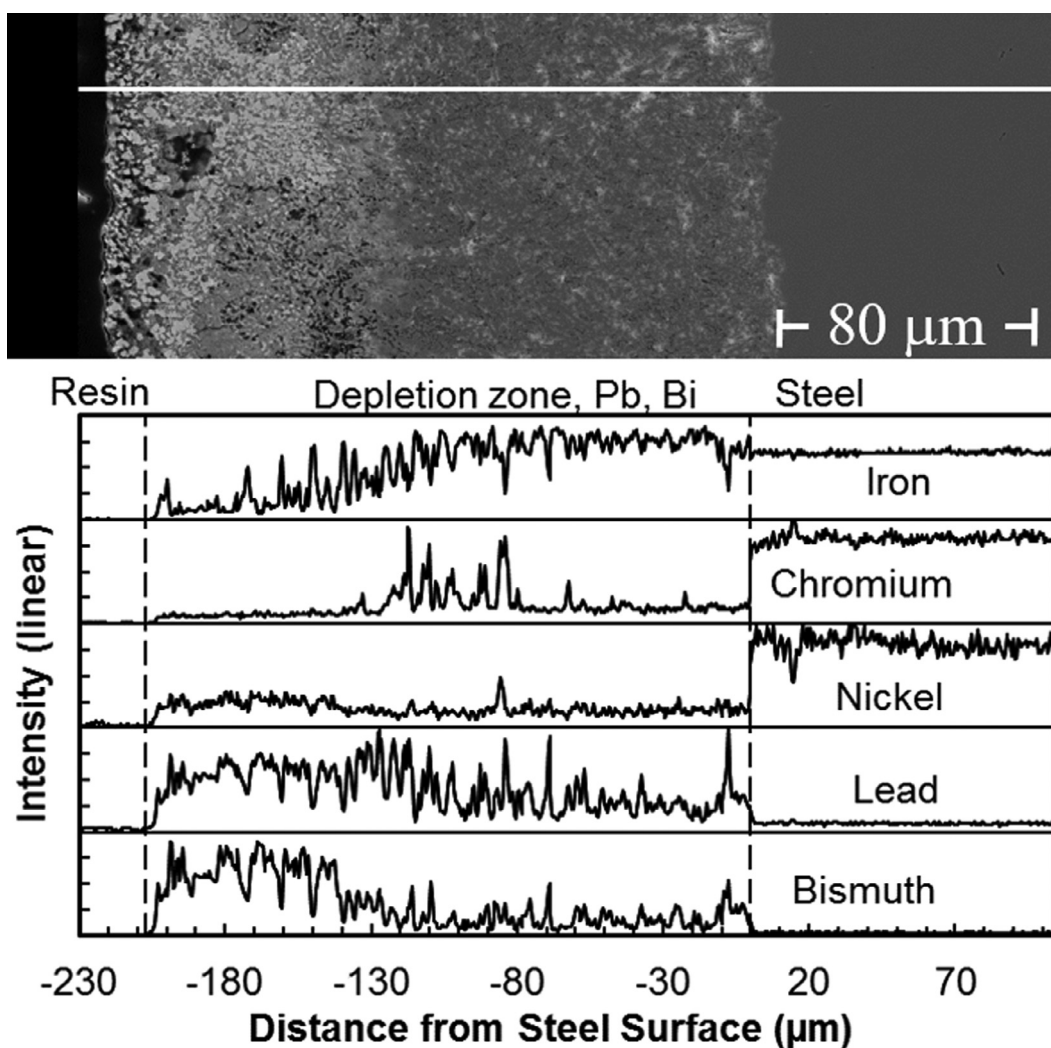

Fig. 11. EDX profile perpendicular to the corrosion scale on the transverse cross-section of 316L tested in LBE with $c_o=1 \times 10^{-7}$–8×10^{-11} wt.% at 550 °C and 300 MPa for 1060 h.
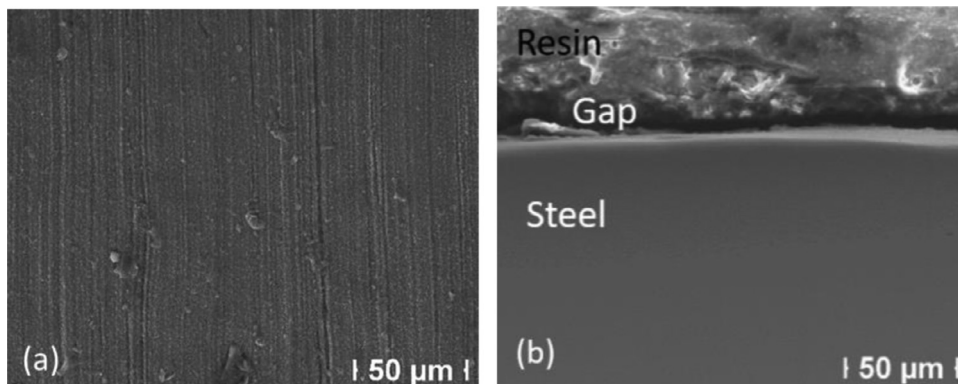
Fig. 12. 316L austenitic steel after creep testing in air at 300 MPa and 550 °C for 1150 h: (a) lateral surface (b) transversal cross-section of the specimen.
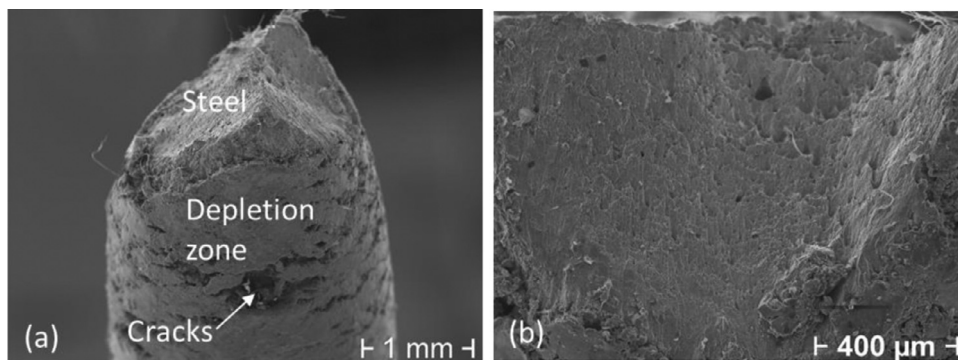
Fig. 13. 316L tested in LBE with $c_o = 1 \times 10^{-6}$ wt.% at 550 °C and 300 MPa for 231 h: (a) part of the specimen close to the fracture, (b) fracture surface with elongated dimples.
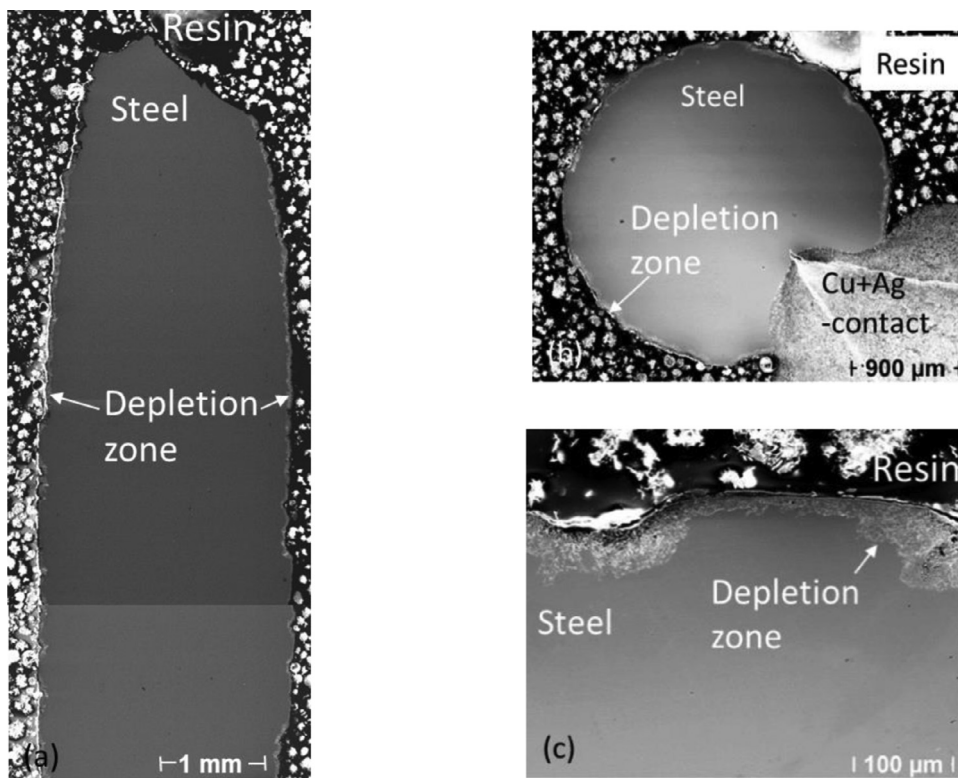

Fig. 14. 316L tested in LBE with $c_o = 1 \times 10^{-6}$ wt.% at 550 °C and 300 MPa for 182 h: (a) longitudinal and (b-c) cross-section of the ruptured specimen.
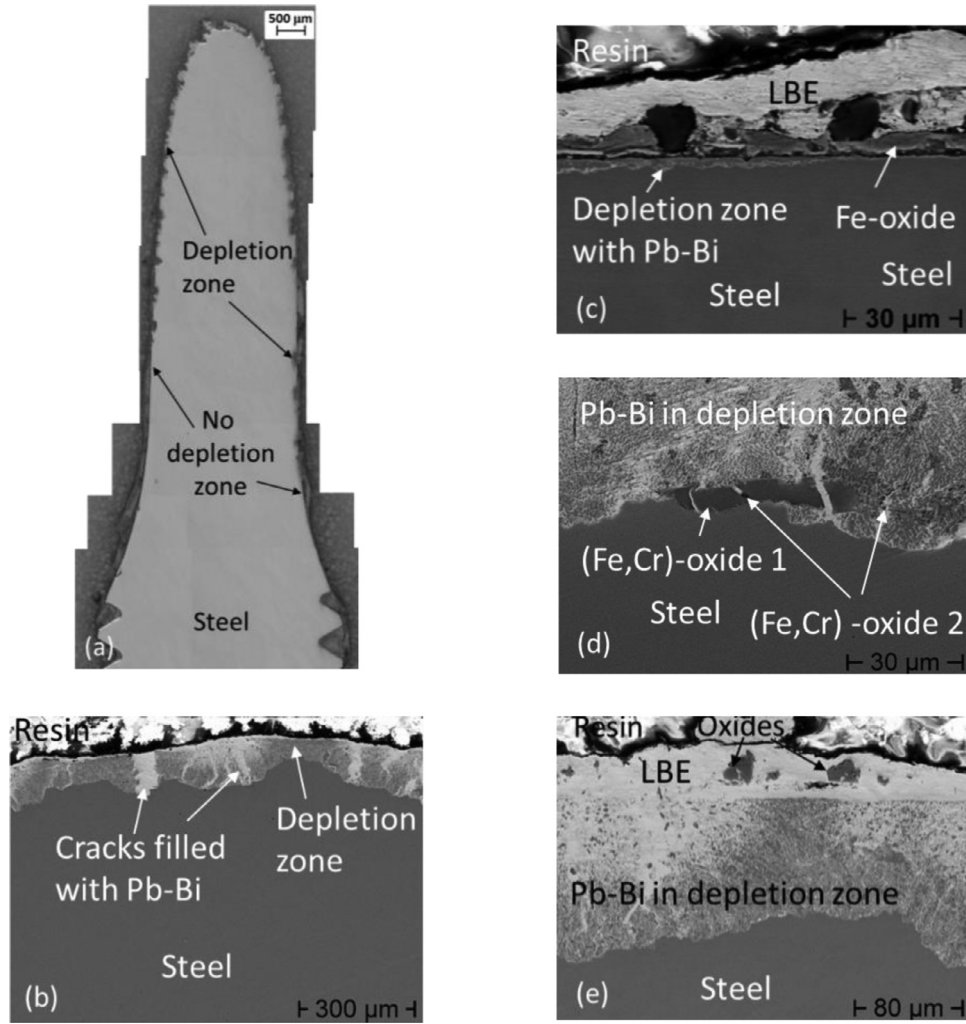
Fig. 15. Longitudinal cross-sections of 316L tested in LBE with $c_o = 1 \times 10^{-6}$ *wt.%* at 550 °C and 300 MPa for 371 h and not cleaned from liquid metal afterwards: (a) along a part of the ruptured specimen, (b) close to failure, (c) close to a screw shoulder, (d-e) between (b) und (c).
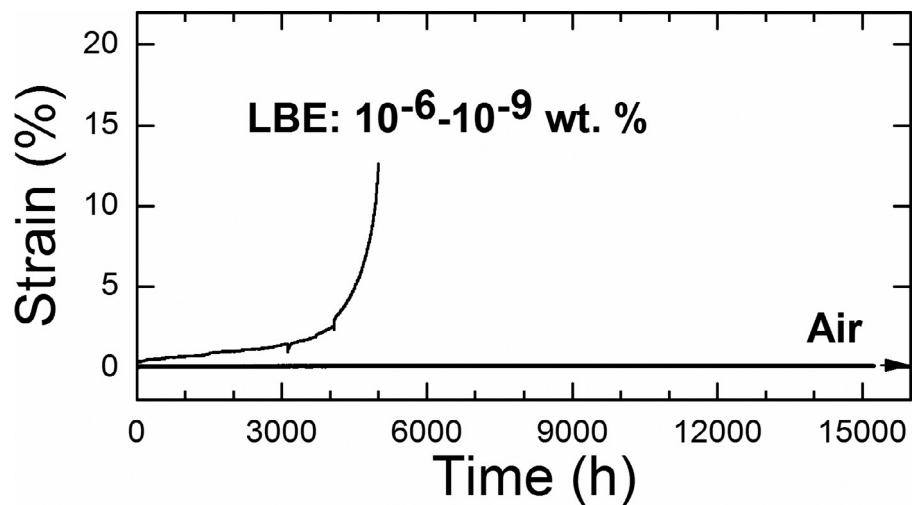

Fig. 16. Strain of 316L ruptured in LBE at $c_o = 10^{-6} - 10^{-9}$ *wt.%* and crept in air at 500 °C. The test in air was stopped after 15,226 h.
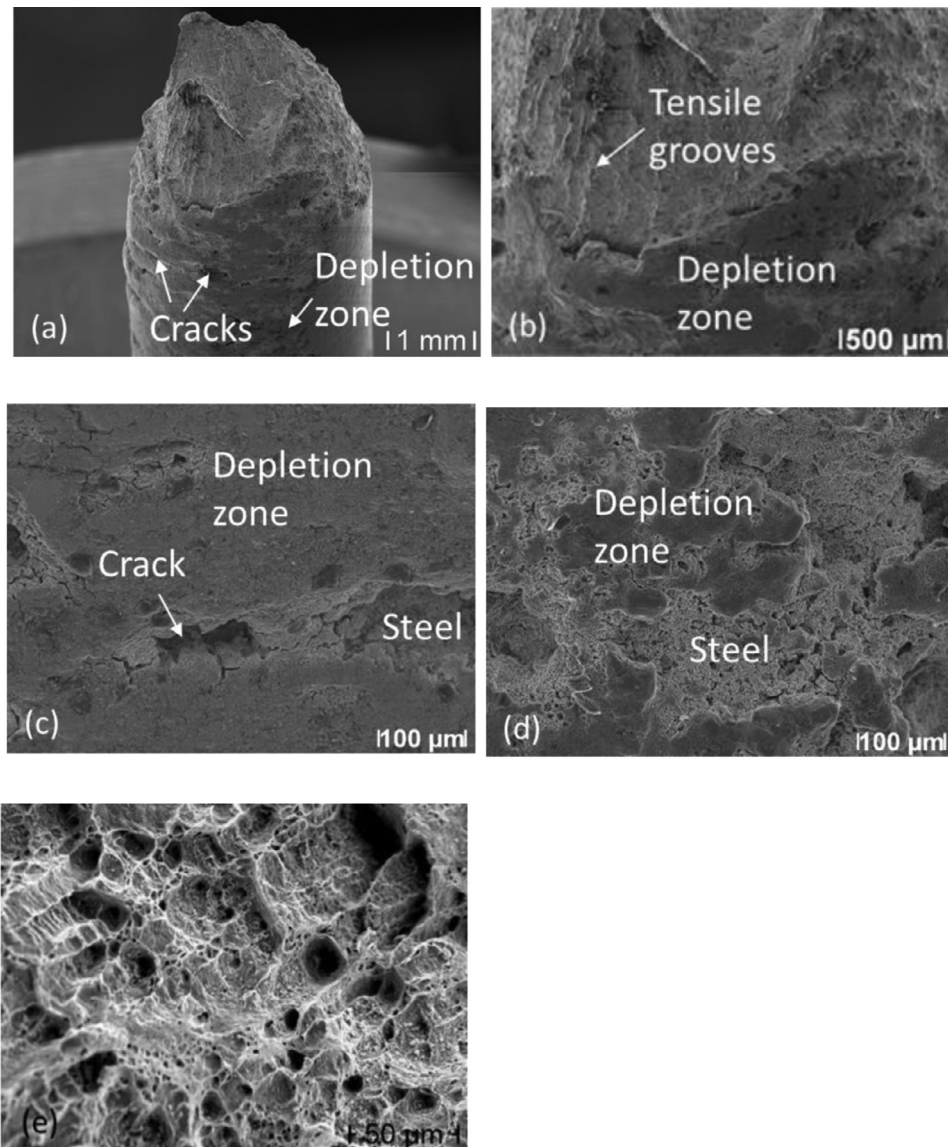
Fig. 17. 316L-sample tested in LBE with $c_o=10^{-8}$–10^{-9} wt.% at 325 MPa and 500 °C, t_R=4996 h: (a) fractured part, (b-d) lateral surface contacted to liquid metal, (e) fractured surface.

An average thickness of the depletion zone is around 81.4 μm (Table 3).

Reference specimen tested in air at 500 °C was intact after 15,226 h. The steel surface is slightly oxidized and exhibits an entireness excepting a minor amount of cracks in an oxidized surface (Fig. 19).

During metallographic study, any relevant microstructural change was not determined in the inner of the steel: elongated lamellas presented through δ-phase in as-received steel have changed neither in size nor in shape. Its amount in the inner of the gauge length is compared on the same surface square before and after the test (Fig. 1a). Any new phase was not determined after creep at 500 °C for 15,226 h.

3.3. 450 °C and 375 MPa

316L tested at 375 MPa and 450 °C is intact in air after 5783 h as well as in LBE with low c_o after 7178 h testing (Fig. 20). Steady-state strain rate for the LBE-specimen is two orders higher than for the air-specimen: $\dot{\varepsilon}_s^r$ =1.5 × 10^{-5} h^{-1} in LBE and $\dot{\varepsilon}_s^r$ =8.8 × 10^{-8} h^{-1} in air (Table 3). The strain-vs.-time curve for the LBE-specimen shows increase in strain with time, while the curve for the air-specimen does not exhibit any significant change in the strain. Therefore, the time corresponding to the transitions from primary to secondary creep, $t_{1,2}$ in LBE is determined around 124.5 h, while $t_{1,2}$ in air cannot be identified with accuracy of the actual creep facility; it cannot be excluded as well that $t_{1,2}$ in air is still not reached.

The 316L-specimen tested in LBE with $c_o=10^{-9}$–10^{-10} wt.% exhibits rough surface on the whole specimen that is corroded and infiltrated with LBE after 7178 h testing (Fig. 21). Dissolution of the steel elements and following infiltration of liquid metal is presented through a pit-type occurrence selective leaching.

The δ-ferrite has not been subjected to any change in chemical content and size during the tests at 450 °C and 375 MPa that was defined with EDX-mapping analysis of composites.

Thickness of a depletion zone formed in LBE with lowering oxygen content at 450 °C is around 53 μm after 7178 h creep testing. The specimen radius formed from the austenitic steel was measured after the experiment to reduce by around 283 μm; material los with a simultenious necking is around 33 % (Table 3).
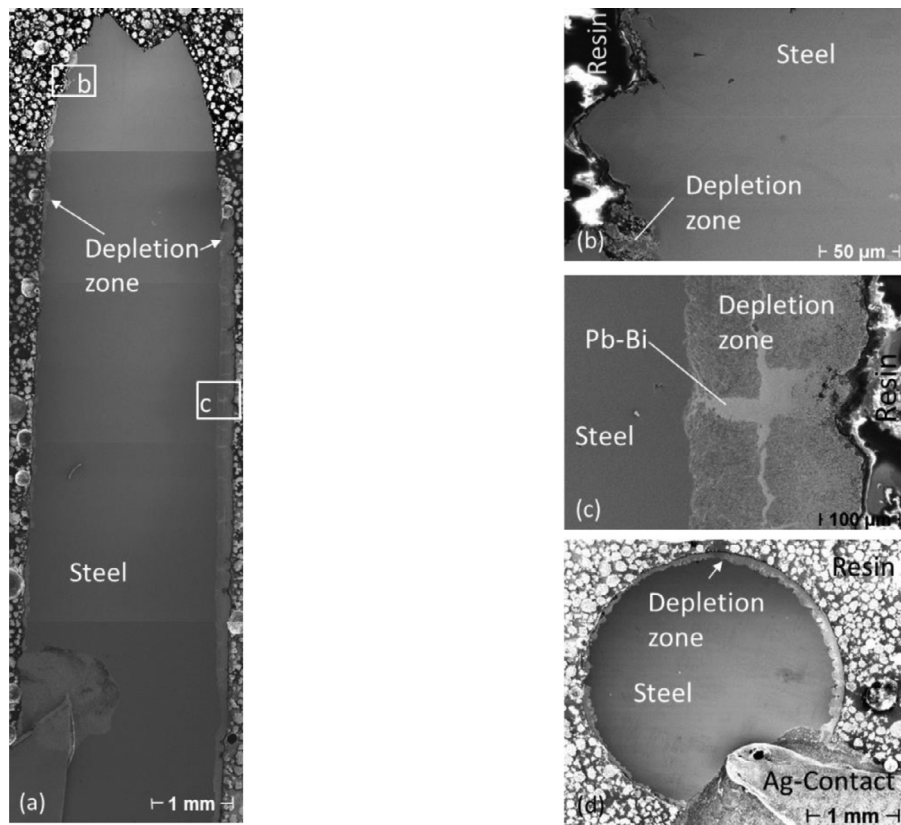
Fig. 18. Longitudinal cross section of 316L tested in LBE with $c_o = 10^{-8} - 10^{-9}$ wt.% at 500 °C and 325 MPa, $t_R = 4996$ h.
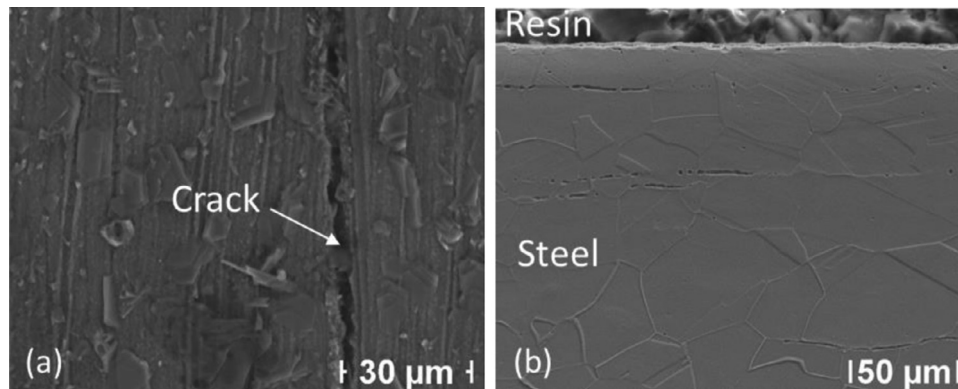

Fig. 19. 316L-sample after the creep test in air at 500 °C and 325 MPa for 15,226 h with a horizontal orientation of tensile direction: (a) lateral steel surface, (b) etched longitudinal cross-section.

During the test in air, the steel surface slightly oxidizes (Fig. 22a). Surface cracks are not observed. Examination with SEM reveals striations perpendicular to the tension direction (Fig. 22b). Any microstructural change was not observed in comparison to as-received material: the δ-ferrite islands are enriched with Cr, and Mo as well as depleted with Fe and Ni in comparison to the steel matrix.

In contrast to the test in LBE, no corrosion scale was observed on the specimen tested at 450 °C in air after 5.783 h testing (Fig. 22a), while a sample radius is reduced on 135.9 μm with a corresponding reduction of the load-bearing cross-section of around 17 %. This indicates that reduction of the radius occurs due to elongation under sress applied during the creep test, while corrosion did not affect significantly on the creep characteristics of the steel. Also, microstructural changes inside of the steel tested in LBE and air at 450 °C for 7178 and 5783 h correspondingly were

not observed by means of SEM. A very low steady-state strain rate of the steel in both media at 450 °C (Table 3) let us to estimate a rupture time still for a long time. But due to dissolution of the steel components in LBE, a higher steady-state strain rate in LBE and a higher reduction of the specimen radius in LBE, one can expect that 316L may ruptured in LBE earlier than in air at 450 °C similar to higher temperatures.

3.4. Discussion

Creep-to-rupture test in LBE at 550 °C with a lowering oxygen content resulted in a considerably reduced the time-to-rupture, t_R in comparison to air. Formation of a thick depletion zone on the steel surface after 1060 h well-observed with LOM and SEM reduces significantly a load-bearing cross-section and results finally in a premature failure of the steel (Fig. 8a,c and Fig. 7). Depletion
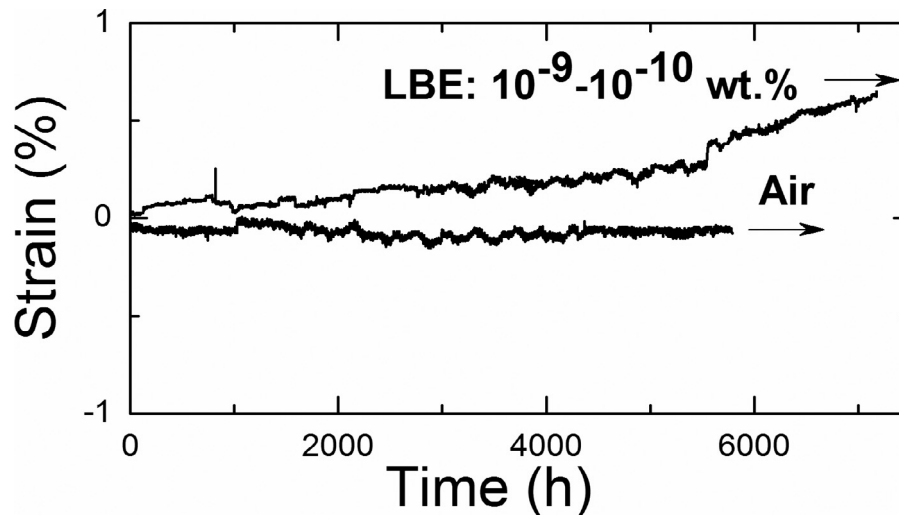
Fig. 20. Strain as a function of time at 450 °C, 375 MPa for 316L in LBE (c_o=10^{-9}–10^{-10} *wt.%*) and air. The tests were stopped after 7178 and 5783 h, respectively.
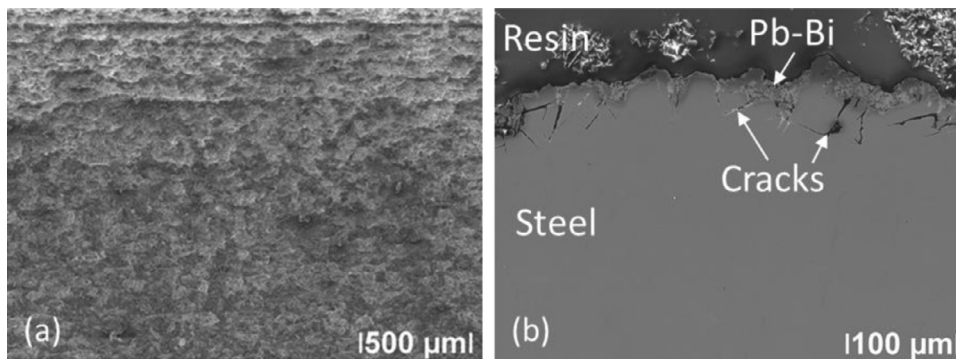

Fig. 21. 316L after the creep test in LBE (c_o =10^{-9}–10^{-11} wt.%) at 450 °C, 375 MPa for 7178 h with a horizontal orientation of tensile direction: (a) lateral surface contacted to liquid metal, (b) non-etched transverse cross-section.
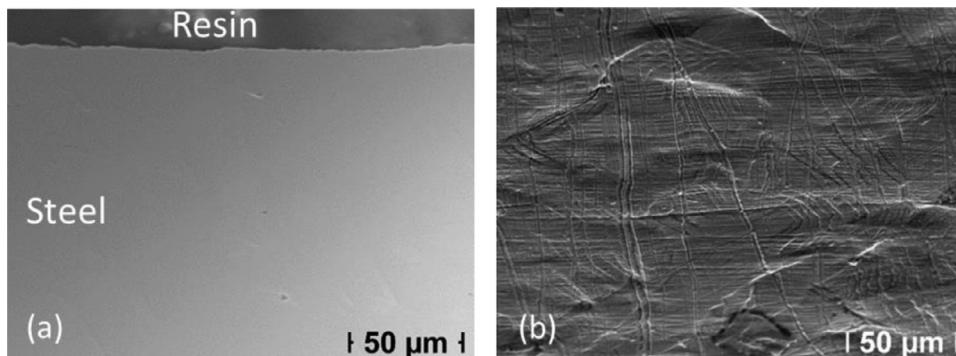

Fig. 22. SEM image of the 316L steel creep test in air at 450 °C, 375 MPa for 5783 h: (a) transverse cross-section and (b) lateral surface of the specimen.

zone forming due to a dissolution of the steel components like Ni, Cr and Fe (Fig. 11) is affected by a temperature. Thickness of the depletion zone depends directly on a temperature: the higher temperature of LBE is, the stronger dissolution dynamics was observed that resulted in a thicker depletion zone on 316L. This general tendency belongs to all LBE-tests with a lowering c_o at 450–550 °C. A thickness of a depletion zone can vary due to complex processes underwent during the testing in LBE as well as affected by a preparation of the specimen for study after the test. So, it is clear demonstrated on the LBE-specimen at 550 °C that a depletion zone is irregular thick along the tensile direction (Fig. 9a). Reducing the test temperature to 500 and 450 °C, a steel surface

dissolves with a time more regular and a depletion zone is observed on the whole specimen along the tensile direction (Figs. 15a and 21a). With a time growing depletion zone becomes less stable and can spall off during the testing as well as during the specimen preparation after the testing and result in a different thickness of the corroded scale like in Fig. 18c. Therefore, some transversal cross-sections of the LBE-specimens exhibit depletion zone, some of them not and it is very irregular on some of them. A thickness of a depletion zone is introduced in Table 3 just for a conceivability of corrosion dynamics for every specimen, because the values do not reflect more complicated processes went during the testing.

Tensile stress can affect corrosion as well, since diffusion of atoms in the steel under stress is assisted. Corrosion data for the 316L steel in the flowing LBE at $c_o=10^{-7}$ wt.% and 450 and 550 °C in Ref. [41] and in static LBE at $c_{o=}10^{-7}$ wt.% and 450–500 °C in Refs. [42,43] and our data support this tendency, but do not explain all data, e.g. at 450 and 550 °C. Moreover, it is needed keep in mind, that begin of ferritisation is affected by an incubation time, so long as oxide layer on the specimen is intact and did not rupture. With a time, the specimen starts to narrow and an oxide layer tears there, so that dissolution of the steel elements towards liquid LBE and LBE attack vice versa take place.

Depletion of the steel with the steel components like nickel, chromium and iron occurs due to strong distinguish in their concentration in the steel and liquid metal [12]. At low c_o, dissolution of the steel starts as far as protective oxide film is destroyed and decelerates with a time. As a consequence a depletion zone grows with a time. Eventually, it comes to a moment, when Ni, Cr and Fe cannot be delivered from the steel so fast as they dissolve from the outer part of the depletion zone into liquid metal. Liquid LBE infiltrates increasingly into vacant positions in the corrosion layer and a depletion zone is destroying consequently with a time (Figs. 10 and 11).

A corrosion scale loses strength; orbital and radial cracks occur within a depletion zone (Figs. 9b and 10a). Thermal creep mechanism occurs inside the steel bulk before the full rupture. The corrosion induced thickness loss causes an increase in effective stress acting on the remaining steel bulk. Before this effective stress exceeds ultimate tensile stress (UTS) of the steel, the typical creep mechanism at elevated temperatures should operate. As corrosion continues, this effective stress may exceed UTS. From this moment on, the deformation of the specimen will migrate to an unstable loading condition similar to the tensile deformation after UTS is reached.

Any evidence that cracks originated within a depletion zone and propagated towards the steel would propagate further into the steel and becomes an origin of the failure was not observed. Higher content of liquid metal in outer part of the depletion scale was reported in the austenitic steel 1.4571 after long-operation of COR-RIDA loop around 66,000 h at 550 °C [12]. Two mechanisms of the steel dissolving (non-selectively or selectively with a supply of dissolving elements to the interface of the depleted solid phase via solid-state diffusion) was proposed to explain porosity of a depletion zone and give a rise of penetration of the corrosive fluid [12].

Oxidation of the 316L in air at 550 and 500 °C determined after 1150 and 15,128 h, correspondingly, is very light: an oxide film is not detected by means of SEM, turning traces are still observed on lateral surface. So, no detrimental effect of air on the steel surface during creep was established.

At 450 °C, a depletion zone forms similarly on the steel surface with a feature that it spreads on whole specimen surface contacted to LBE and dissolves irregularly in liquid LBE during 7178 h testing. As result the specimen looks rough on the whole surface (Fig. 21a). Comparing the steel surfaces in LBE and air at 450 °C, striations are observed to grow in air perpendicular to the tensile direction and no cracks are found as well no visible oxidation are established. The striation could result from movement of dislocation lines on the surface along tensile direction under loading. Since no cracks appeared on the surface, a low steady-state creep rate without a sign to reach $t_{2,3}$ characterize the specimen, one can expect a long testing time before the specimen ruptures. Furthermore, similar to 550 and 500 °C, it is expected that at 450 °C, the steel in LBE will rupture earlier than in air by the same other conditions.

Increasing an oxygen dissolved in LBE to 10^{-6} wt.% at 550 °C did not result in a higher time-to-rupture. Three tests showed even shorter t_R than at $c_o=10^{-7}$–10^{-11} wt.%. In spite of stable ox-

ides with Fe and Cr could form at these conditions [39], three specimens exhibit a depletion zone on the steel. The specimen that was not cleaned from LBE-rests after the testing exhibits oxides at steel/depletion zone interface, in a depletion zone, on the specimen surface as well outside the specimen in solidified LBE (Fig. 15c-e).

In corrosion tests in flowing LBE at 550 °C and $\sim 10^{-7}$ wt.% dissolved oxygen, a depletion zone was reported after 2.011 h, while at shorter testing times a thin oxide film protects the steel surface from the corrosion [15]. In static LBE at 500 °C and low c_o ($<10^{-13}$ wt.%), dissolution was specified to be a main corrosion mechanism of 316L [43]. In Refs. [42,43] it was shown that a thin oxide layer forms on 316L and the steel begins to dissolve at 450 °C and c_o in-between 10^{-6} and 10^{-7} wt.%. Namely, protective properties of the formed oxide film formed at 450–550 °C and $c_o \leq 10^{-6}$ wt.% is inherently not protective with respect to the dissolution of Ni by liquid metal or becomes not protective with time because of formation of defects favoring local leaching of Ni and/or Cr even without loading [15]. Based on these reports, two factors, namely loading and an interaction of the steel with LBE have to facilitate formation of a depletion zone and oxide layer on 316L observed simultaneously after creep-to-rupture test at 550 °C and 10^{-6} wt.% dissolved oxygen. Loading the specimen results in a faster tearing of a thin oxide layer on the 316L surface than it is expected without loading. A following contact of a virgin steel surface to LBE can lead to a local oxidation of the surface as well as to a dissolution of the steel elements as soon as oxygen content in LBE not high enough to form oxides. Dissolved steel elements such as Cr, Fe can oxidize in liquid LBE due to locally sufficient supply of oxygen. Formation of oxides and oxide layer were observed locally in a depletion zone and at steel/depletion zone interface, and on the top of depletion zone. So, liquid LBE infiltrated into depletion zone and deeper, close to the specimen surface has locally enough oxygen to oxidize the steel elements. Finally, dissolution process becomes more preferential with a time than oxidation at 550 °C and 10^{-6} wt.% dissolved oxygen. Hence, a dissolution of the 316L austenitic steel is a main degradation factor at all test temperatures and oxygen dissolved in LBE. Oxide layer if it forms at $c_o=10^{-6}$ wt.% does not stable enough under loading to protect the steel from a dissolution. A possible running of two different corrosion processes results finally in a stronger degradation of the steel surface and consequently in a shorter time-to-rupture, t_R. Corrosion mechanism at $c_o=10^{-6}$ wt.% resulted in a shorter time-to-rupture than at lower oxygen dissolved in LBE is not obvious and needs to be studied in details.

All failures studied after LBE-tests show a ductile mode. Any feature for liquid metal embrittlement (LME) was not observed on 316L tested in LBE. Any change in microstructure of the steel volume was determined after short- and long-term testing. The δ-phase detected in as-received material exhibits any transformation in its shape, amount, size and composition.

Necking, Z and strain at rupture, ε_r^R of 316L in LBE are in the ranges of 29–43 % and of 13–20%, correspondingly. Steady-state strain rate, $\dot{\varepsilon}_s^r$ is one order higher in LBE than in air at corresponding test temperatures. Transformation time from secondary to tertiary creep stage, $t_{2,3}$ in LBE increases by reducing of test temperature as well as by increasing of c_o to 10^{-6} wt.% at 550 °C. Steel dissolution in LBE as a main degradation factor defines a higher rate of ferritisation and, consequently resulted in reducing of load-bearing cross-section: (i) a steady-state strain rate is in generally one-two orders higher in LBE than in air (with an exception for 550 °C with low c_o) as well as (ii) a shorter $t_{2,3}$ resulted in a shorter t_R of the steel (Fig. 7 and Table 3). Strain-at-rupture, ε_r^R at 550 °C is in the range of 14.2–29.3 %, at 500 °C it is 13.0% and is on the lowest border of the 550 °C-range.

4. Conclusion

The 316L austenitic steel exhibits a premature failure during creep-to-rupture in LBE in comparison to air, especially at 500 and 550 °C. This can be anticipated also for 450 °C, 375 MPa and 10^{-9}–10^{-11} wt.% dissolved oxygen although the last test was not performed until rupture.

The obvious reason is corrosion, i.e. selective leaching of steel elements such as nickel and associated reduction of load-bearing cross-section. Protective oxide survives only locally, e.g. at the specimen ends. Failure mode is always ductile.

Declaration of Competing Interest

The authors declare that they have no known competing financial interests or personal relationships that could have appeared to influence the work reported in this paper.

CRediT authorship contribution statement

Mariya Yurechko: Conceptualization, Methodology, Investigation, Formal analysis, Visualization, Writing – original draft, Writing – review & editing. **Aleksandr Skrypnik:** Resources, Investigation, Data curation. **Olaf Wedemeyer:** Software. **Jürgen Konys:** Funding acquisition, Project administration. **Carsten Schroer:** Supervision, Conceptualization, Methodology, Formal analysis, Writing – original draft, Writing – review & editing.

Acknowledgement

References

[1] C. Fazio, V.P. Sobolev, A. Aerts, S. Gavrilov, K. Lambrinou, P. Schuurmans, A. Gessi, P. Agostini, A. Ciampichetti, L. Martinelli, S. Gosse, F. Balbaud-Celerier, J.L. Courouau, A. Terlain, N. Li, H. Glasbrenner, J. Neuhausen, S. Heinitz, L. Zanini, Y. Dai, M. Jolkkonen, Y. Kurata, T. Obara, N. Thiolliere, F.J. Martin-Munoz, A. Heinzel, A. Weisenburger, G. Mueller, G. Schumacher, A. Jianu, J. Pacio, L. Marocco, R. Stieglitz, T. Wetzel, M. Daubner, K. Litfin, J.B. Vogt, I. Proriol-Serre, D. Gorse, S. Eckert, F. Stefani, D. Buchenau, T. Wondrak, I.S. Hwang, Handbook on lead-bismuth eutectic alloy and lead properties, materials compatibility, thermal-hydraulics and technologies, Nuclear Energy Agency (NEA), Issy-les-Moulineaux, France, 2015.
[2] Int. Atomic Energy Agency (IAEA), Power Reactors and Sub-Critical Blanket Systems with Lead and Lead-Bismuth as Coolant and/or Target Material, IAEA TEC-DOC-1348, Vienna, Austria, 2003.
[3] F. Barbier, A. Rusanov, Corrosion behavior of steels in flowing lead-bismuth, J. Nucl. Mater. 296 (2001) 231–236, doi:10.1016/S0022-3115(01)00521-9.
[4] C. Fazio, I. Ricapito, G. Scaddozzo, G. Benamati, Corrosion behaviour of steels and refractory metals and tensile features of steels exposed to flowing PbBi in the LECOR loop, J. Nucl. Mater. 318 (2003) 325–332, doi:10.1016/S0022-3115(03)00009-6.
[5] G. Benamati, C. Fazio, H. Piankova, A. Rusanov, Temperature effect on the corrosion mechanism of austenitic and martensitic steels in lead-bismuth, J. Nucl. Mater. 301 (2002) 23–27, doi:10.1016/S0022-3115(01)00723-1.
[6] G. Mueller, A. Heinzel, J. Konys, G. Schumacher, A. Weisenburger, F. Zimmermann, V. Engelko, A. Rusanov, V. Markov, Results of steel corrosion tests in flowing liquid Pb/Bi at 420–600°C after 2000h, J. Nucl. Mater. 301 (2002) 40–46, doi:10.1016/S0022-3115(01)00725-5.
[7] K. Kikuchi, Y. Kurata, S. Saito, M. Futakawa, T. Sasa, H. Oigawa, E. Wakai, K. Miura, Corrosion–erosion test of SS316 in flowing Pb-Bi, J. Nucl. Mater. 318 (2003) 348–354, doi:10.1016/S0022-3115(03)00017-5.
[8] F.J. Martin-Munoz, L. Soler-Crespo, D. Gomez-Briceno, Corrosion behaviour of martensitic and austenitic steels in flowing lead-bismuth eutectic, J. Nucl. Mater. 416 (2011) 87–93, doi:10.1016/j.jnucmat.2011.01.108.
[9] L. Soler, F.J. Martin, F. Hernandez, D. Gomez-Briceno, Corrosion of stainless steels in lead-bismuth eutectic up to 600°C, J. Nucl. Mater. 335 (2004) 174–179, doi:10.1016/j.jnucmat.2004.07.012.
[10] F. Gnecco, E. Ricci, C. Bottino, A. Passerone, Corrosion behaviour of steels in lead-bismuth at 823K, J. Nucl. Mater. 335 (2004) 185–188, doi:10.1016/j.jnucmat.2004.07.013.
[11] Y. Kurata, M. Futakawa, S. Saito, Corrosion behavior of steels in liquid lead-bismuth with low oxygen concentrations, J. Nucl. Mater. 373 (2008) 164–178, doi:10.1016/j.jnucmat.2007.05.051.
[12] C. Schroer, O. Wedemeyer, J. Novotny, A. Skrypnik, J. Konys, Selective leaching of nickel and chromium from Type 316 austenitic steel in oxygen-containing lead-bismuth eutectic (LBE), Corr. Sci. 84 (2014) 113–124, doi:10.1016/j.corsci.2014.03.016.
[13] C. Schroer, E. Nold, J. Konys, Micro-analysis of 316L stainless-steel after long-term exposure to lead-bismuth eutectic at 550°C, EUROCORR 2009, European Federation of Corrosion (EFC), Nice, France, 2009 paper No. 8026, released on CD.
[14] J. Zhang, A review of steel corrosion by liquid lead and lead-bismuth, Corr. Sci. 51 (2009) 1207–1227, doi:10.1016/j.corsci.2009.03.013.
[15] V. Tsisar, C. Schroer, O. Wedemeyer, A. Skrypnik, J. Konys, Corrosion behavior of austenitic steels 1.4970, 316L and 1.4571 in flowing LBE at 450 and 550°C with 10^{-7} mass% dissolved oxygen, J. Nucl. Mater. 454 (2014) 332–342, doi:10.1016/j.jnucmat.2014.08.024.
[16] W.D. Manly, Fundamentals of Liquid Metal Corrosion, Corrosion 12 (1956) 46–52, doi:10.5006/0010-9312-12.7.46.
[17] M. Navas, R. Hernandez, Compatibility of structural materials with lead and lead bismuth eutectic for CSP applications, in: AIP Conf. Proc. SolarPACES 2017, Santiago, Chile, Sept. 27-29, 2017, 2033, 2018, doi:10.1063/1.5067237.
[18] Y. Kurata, S. Saito, Temperature Dependence of Corrosion of Ferritic/Martensitic and Austenitic Steels in Liquid Lead-Bismuth Eutectic, Mater. Trans. 50 (2009) 2410–2417, doi:10.2320/matertrans.M2009173.
[19] K. Lambrinou, E. Charalampopoulou, T. van der Donck, R. Delville, D. Schryvers, Dissolution corrosion of 316L austenitic stainless steels in contact with static liquid lead-bismuth eutectic (LBE) at 500°C, J. Nucl. Mater. 490 (2017) 9–27, doi:10.1016/j.jnucmat.2017.04.004.
[20] E.E. Glickman, Mechanism of liquid metal embrittlement by simple experiments: from atomistics to life-time, in: J. Lépinoux, D. Mazière, V. Pontikis, G. Saada (Eds.), Multiscale Phenomena in Plasticity: From Experiments to Phenomenology, Modelling and Materials Engineering, Springer Netherlands, Dordrecht, 2000, pp. 383–402.
[21] V.V. Popovich, I.G. Dmukhovskaya, Rebinder effect in the fracture of Armco iron in liquid metals, Mater. Sci. 14 (1979) 365–370, doi:10.1007/BF01154711.
[22] V.Y. Abramov, S.N. Bozin, O.I. Eliseeva, G.M. Kalinin, V.I. Kalyandruk, E.M. Lytyi, Influence of a lead melt on plastic deformation of high-alloyed heat-resistant steels, Mater. Sci. (1994) 465–469.
[23] B. Long, Y. Dai, N. Baluc, Investigation of liquid LBE embrittlement effects on irradiated ferritic/martensitic steels by slow-strain-rate tensile tests, J. Nucl. Mater. 431 (2012) 85–90, doi:10.1016/j.jnucmat.2011.11.036.
[24] X. Gong, P. Marmy, Y. Yin, The role of oxide films in preventing liquid metal embrittlement of T91 steel exposed to liquid lead-bismuth eutectic, J. Nucl. Mater. 509 (2018) 401–407, doi:10.1016/j.jnucmat.2018.07.018.
[25] X. Gong, P. Marmy, A. Volodin, B. Amin-Ahmadi, L. Qin, D. Schryvers, S. Gavrilov, E. Stergar, B. Verlinden, M. Wevers, M. Seefeldt, Multiscale investigation of quasi-brittle fracture characteristics in a 9Cr–1Mo ferritic–martensitic steel embrittled by liquid lead–bismuth under low cycle fatigue, Corros. Sci. 102 (2016) 137–152, doi:10.1016/j.corsci.2015.10.003.
[26] A. Strafella, A. Coglitore, E. Salernitano, Creep behaviour of 15-15Ti(Si) austenitic steel in air and in liquid lead at 550°C, Procedia Struct. Integrity 3 (2017) 484–497, doi:10.1016/j.prostr.2017.04.061.
[27] X. Gong, Z. Yang, Y. Deng, J. Xiao, H. Wang, Z. Yu, Y. Yin, Creep failure of a solution-annealed 15-15Ti steel exposed to stagnant lead-bismuth eutectic at 550 and 600°C, Mater. Sci. Eng. A 798 (2020) 140230, doi:10.1016/j.msea.2020.140230.
[28] E. Stergar, S.G. Eremin, S. Gavrilov, M. Lambrecht, O. Makarov, V. Iakovlev, Influence of LBE long term exposure and simultaneous fast neutron irradiation on the mechanical properties of T91 and 316L, J. Nucl. Mater. 473 (2016) 28–34, doi:10.1016/j.jnucmat.2016.02.008.
[29] Z. Hamouche-Hadjem, T. Auger, I. Guillot, D. Gorse, Susceptibility to LME of 316L and T91 steels by LBE: effect of strain rate, J. Nucl. Mater. 376 (2008) 317–321, doi:10.1016/j.jnucmat.2008.02.031.
[30] G. Coen, J. van den Bosch, A. Almazouzi, J. Degrieck, Investigation of the effect of lead-bismuth eutectic on the fracture properties of T91 and 316L, J. Nucl. Mater. 398 (2010) 122–128, doi:10.1016/j.jnucmat.2009.10.021.
[31] M. Chocholousek, E. Stergar, X. Gong, P. Marmy, S. Gavrilov, F. Ersoy, M. Yurechko-Hussy, C. Schroer, J. Konys, J.-B. Vogt, I. Proriol-Serre, T. Auger, B. Barkia, Z. Spirit, F. Di Gabriele, A. Hojná, D5.42: Report for mech./microstr. character. of environ. assisted degrade. effects of steels in lead alloys and assess. Of environm. degrad. effects on perf. Of struct. and funct. comp. of MYRRHA ADS & LFR. MatISSE – Contract Number: 604862, FP7-Fission-2013, 2018.
[32] A.F. Padilha, C.F. Tavares, M.A. Martorano, Delta Ferrite Formation in Austenitic Stainless Steel Castings, MSF 730-732, 2012, pp. 733–738, doi:10.4028/www.scientific.net/MSF.730-732.733.
[33] A.L. Schaeffler, Constitution diagram for stainless steel weld metal, Metal Progress 56 (11) (1949) 680-680B.
[34] ISO 204:2009-10, Metallic Materials - Uniaxial Creep Testing in Tension - Method of Test (ISO 204:2009), German Version EN ISO 204:2009-10, Beuth, Berlin, Germany, 2009.
[35] J. van den Bosch, A. Almazouzi, Procurement and Characterisation of T91 and SS316L plates, EUROTRANS FI6W-CT-2004-516520, R-4197, SCK-CEN, Mol, Belgium, 2005.

[36] M. Yurechko, C. Schroer, O. Wedemeyer, A. Skrypnik, J. Konys, Creep-to-rupture of 9%Cr steel T91 in air and oxygen-controlled lead at 650°C, J. Nucl. Mater. 419 (2011) 320–328, doi:10.1016/j.jnucmat.2011.05.034.

[37] C. Schroer, O. Wedemeyer, J. Konys, Gas/liquid oxygen-transfer to flowing lead alloys, Nucl. Eng. Des. 241 (2011) 1310–1318, doi:10.1016/j.nucengdes.2010.06.047.

[38] M. Yurechko, C. Schroer, A. Skrypnik, O. Wedemeyer, V. Tsisar, J. Konys, Steel T91 subjected to static stress in lead-bismuth eutectic at 450–550°C and low oxygen concentration, J. Nucl. Mater. 512 (2018) 423–439, doi:10.1016/j.jnucmat.2018.09.056.

[39] C. Schroer, J. Konys, Physical Chemistry of Corrosion and Oxygen Control in Liquid Lead and Lead-Bismuth Eutectic, FZKA-7634, Karlsruhe Institute of Technology (KIT), Karlsruhe, Germany, 2007 https://publikationen.bibliothek.kit.edu/270069895.

[40] M. Rieth, A. Falkenstein, P. Graf, S. Heger, U. Jäntsch, M. Klimiankou, E. Materna-Morris, H. Zimmermann, Creep of the Austenitic Steel AISI 316 L(N): Experiments and Models, FZKA-7065, Karlsruhe Institute of Technology

(KIT), Karlsruhe, Germany, 2004 http://bibliothek.fzk.de/zb/berichte/FZKA7065.pdf.

[41] V. Tsisar, C. Schroer, O. Wedemeyer, A. Skrypnik, J. Konys, Long-term corrosion of austenitic steels in flowing LBE at 400°C and 10^{-7} mass% dissolved oxygen in comparison with 450 and 550°C, J. Nucl. Mater. 468 (2016) 305–312, doi:10.1016/j.jnucmat.2015.09.027.

[42] O. Klok, K. Lambrinou, S. Gavrilov, J. Lim, I. de Graeve, Effect of lead-bismuth eutectic oxygen concentration on the onset of dissolution corrosion in 316L austenitic stainless steel at 450°C, J. Nucl. Eng. Rad. Sci. 4 (2018) 1331, doi:10.1115/1.4039598.

[43] O. Klok, K. Lambrinou, S. Gavrilov, E. Stergar, J. Lim, T. van der Donck, W. van Renterghem, I. de Graeve, Effect of deformation twinning on dissolution corrosion of 316L stainless steels in contact with static liquid lead-bismuth eutectic (LBE) at 500°C, J. Nucl. Mater. 510 (2018) 556–567, doi:10.1016/j.jnucmat.2018.08.030.